

Review of magnons in van der Waals materials: From fundamental physics to frontiers

Zhen-Nan Wang(王震南), Yan-Pei Lv(吕延培), Hao-Nan Chang(常浩男), and Jun Zhang(张俊)
Citation: Chin. Phys. B, 2025, 34 (**10**): 107201. DOI: 10.1088/1674-1056/ade06c
http://cpb.iphy.ac.cn; http://iopscience.iop.org/cpb

What follows is a list of articles you may be interested in

Nonreciprocal microwave-optical entanglement in Kerr-modified cavity optomagnomechanics

Ming-Yue Liu(刘明月), Yuan Gong(龚媛), Jiaojiao Chen(陈姣姣), Yan-Wei Wang(王艳伟), and Wei Xiong(熊伟)
Chin. Phys. B, 2025, 34 (**5**): 057202. DOI: 10.1088/1674-1056/adb735

Magnon-magnon coupling in noncollinear synthetic antiferromagnets

Tengfei Zhang(张腾飞), Quwen Wang(王曲文), Min Chen(陈敏), Jie Dong(董洁), Qian Zhao(赵乾), Zimu Li(李子木), Qingfang Liu(刘青芳), Jianbo Wang(王建波), and Jinwu Wei(魏晋武)
Chin. Phys. B, 2025, 34 (**5**): 057201. DOI: 10.1088/1674-1056/adb26b

Strain-dependent resistance and giant gauge factor in monolayer WSe_2

Mao-Sen Qin(秦茂森), Xing-Guo Ye(叶兴国), Peng-Fei Zhu(朱鹏飞), Wen-Zheng Xu(徐文正), Jing Liang(梁晶), Kaihui Liu(刘开辉), and Zhi-Min Liao(廖志敏)
Chin. Phys. B, 2021, 30 (**9**): 097203. DOI: 10.1088/1674-1056/ac11d2

Role of Ag microalloying on glass forming ability and crystallization kinetics of ZrCoAgAlNi amorphous alloy

A Surendar, K Geetha, C Rajan, and M Alaazim
Chin. Phys. B, 2021, 30 (**1**): 017201. DOI: 10.1088/1674-1056/abb65e

Spin Seebeck effect and spin Hall magnetoresistance in the $Pt/Y_3Fe_5O_{12}$ heterostructure under laser-heating

Shuanhu Wang(王拴虎), Gang Li(李刚), Jianyuan Wang(王建元), Yingyi Tian(田颖异), Hongrui Zhang(张洪瑞), Lvkuan Zou(邹吕宽), Jirong Sun(孙继荣), Kexin Jin(金克新)
Chin. Phys. B, 2018, 27 (**11**): 117201. DOI: 10.1088/1674-1056/27/11/117201

TOPICAL REVIEW — Advanced magnonics

Review of magnons in van der Waals materials: From fundamental physics to frontiers

Zhen-Nan Wang(王震南)[1,2], Yan-Pei Lv(吕延培)[1,2], Hao-Nan Chang(常浩男)[1,2], and Jun Zhang(张俊)[1,2,†]

[1] *State Key Laboratory of Semiconductor Physics and Chip Technologies, Institute of Semiconductors, Chinese Academy of Sciences, Beijing* 100083, *China*

[2] *Center of Materials Science and Optoelectronics Engineering, University of Chinese Academy of Sciences, Beijing* 100049, *China*

(Received 31 March 2025; revised manuscript received 23 May 2025; accepted manuscript online 4 June 2025)

The magnons (the quanta of collective spin-wave excitations) in two-dimensional van der Waals (vdW) magnets exhibit some intriguing characteristics, such as spin Nernst effect, topological magnons, Weyl magnons, moiré magnons, magnon valley Hall effect, etc., and can be regulated through approaches such as stacking, electric doping, pressure, strain and twisting, opening unprecedented avenues to explore fundamental magnetic physics and spin-based technologies. Over the past few years, intense research efforts have been invested in unraveling magnon properties in vdW materials. This review comprehensively summarizes recent advancements in understanding magnons in vdW magnetic systems, spanning fundamental theories and experimental frontiers. It also introduces the experimental techniques widely used in this field, including inelastic neutron scattering, Raman/Brillouin spectroscopy, time-resolved spectroscopy and inelastic magneto-tunneling spectroscopy, and discusses the coupling between magnons and other excitations, such as phonons and excitons.

Keywords: van der Waals materials, magnons, spin waves, low-dimensional magnetism

PACS: 72.10.Di, 33.20.Fb, 07.55.Db

DOI: 10.1088/1674-1056/ade06c **CSTR:** 32038.14.CPB.ade06c

1. Introduction

The discovery of two-dimensional (2D) van der Waals (vdW) materials has revolutionized condensed matter physics, offering unprecedented opportunities to explore emergent quantum phenomena in atomically thin systems.[1–7] Among these, vdW magnets bring another surge of research, which began at the observation of the monolayer antiferromagnet (AFM) $FePS_3$ in 2016 and the monolayer ferromagnet (FM) CrI_3, $Cr_2Ge_2Te_6$ in 2017.[8–10] To date, many other vdW magnets have been experimentally discovered, including CrSBr,[11–13] $NiPS_3$,[14–16] $MnBi_2Te_4$,[17–19] and others. Unlike 3D magnets, 2D vdW magnets have theoretically predicted intriguing phenomena, including the spin Nernst effect,[20] topological magnons,[21,22] Weyl magnons,[23] moiré magnons,[24] and the magnon valley Hall effect.[25] As a layered material coupled with van der Waals forces, the vdW magnets can be regulated through approaches such as stacking, electrostatic doping, pressure, strain and twisting, which makes vdW magnets a versatile platform for exploring low-dimensional magnetism and enabling new functionalities in spintronics and quantum technologies.[3,4,7]

Spin wave is an oscillatory collective excitation of the magnetic moments in ferromagnetic or antiferromagnetic media, whose quanta is magnon, a bosonic quasiparticle.[26–28] Magnons carry only spins and are independent of charge, therefore do not cause Ohmic losses,[29] for which magnons can be used to realize low-power transmission. Besides, magnons maintain the characteristics such as low-THz frequency range,[30,31] transferring over macroscopic distances,[32] and access to wave-based computing concepts.[33] These advantages make magnons good information carriers. The emerging field that refers to information transport and processing by magnons is known as magnonics.[29] Several effective approaches for manipulating magnons — including spin-transfer torques and voltage-controlled magnetic anisotropy — rely on interfacial effects, making thinner devices more effective.[34] However, it is challenging to fabricate three-dimensional magnets like yttrium iron garnet (YIG) into high-quality ultrathin films due to the surface roughness and disorder.[35] The vdW materials provide promising solutions to solve this problem, then are critical for next-generation computing architectures.

In this review, we first provide a brief overview of magnons in vdW magnets and their fundamental theory in Section 2. Then, we summarize recent experimental results of magnons in some vdW magnets in Section 3. Specifically, we review some commonly used experimental techniques for detecting magnons in vdW magnets in Section 4 and discuss the interaction between magnons and other quasiparticles of materials in section 5. Finally, we conclude with a discussion of future perspectives and opportunities in this field.

†Corresponding author. E-mail: zhangjwill@semi.ac.cn

© 2025 Chinese Physical Society and IOP Publishing Ltd. All rights, including for text and data mining, AI training, and similar technologies, are reserved.

2. Fundamental theory of magnons in vdW magnets

2.1. Hamiltonian of 2D magnet systems

There are various crystalline structures and distinct spin coupling mechanisms in different van der Waals magnets. Hence, the theoretical models for different vdW magnets are different. Let us introduce the various Hamiltonian models of vdW magnets.

For most of the vdW magnet, the Hamiltonian can be split with[1]

$$\mathcal{H} = H_{\rm ex} + \mathcal{H}_{\rm a} + \mathcal{H}_{\rm DM} + \mathcal{H}_{\rm Kitaev}, \tag{1}$$

where $\mathcal{H}_{\rm ex} = -\sum_{i<j} J_{ij} \hat{\boldsymbol{S}}_i \cdot \hat{\boldsymbol{S}}_j$ is the Heisenberg exchange interaction Hamiltonian. $\hat{\boldsymbol{S}}_i$ is the spin at the i site in the lattice of magnets. J_{ij} is the Heisenberg exchange coupling strength between i site and j site. Positive exchange coupling makes two spins parallel ($J_{ij} > 0$, ferromagnetic coupling), and negative exchange coupling makes two spins antiparallel ($J_{ij} < 0$, antiferromagnetic coupling). $\mathcal{H}_{\rm a} = -A_\alpha \left(\hat{S}_i^\alpha\right)^2$ is the magnetic anisotropy Hamiltonian. A_α is the anisotropy parameter along α axis ($\alpha = x$, y or z), and $\hat{S}_i^\alpha$ is the α component of the spin at i site. This term selects a specific direction preference for spins. It may arise from various aspects, such as exchange anisotropy or magnetocrystalline anisotropy, etc.[1] $\mathcal{H}_{\rm DM} = -\boldsymbol{D}_{ij} \cdot \left(\hat{\boldsymbol{S}}_i \times \hat{\boldsymbol{S}}_j\right)$ is Dzyaloshinskii–Moriya interaction (DMI) Hamiltonian. $\boldsymbol{D}_{ij}$ is Dzyaloshinskii vector, pointing along a high-symmetry direction of the magnetic crystals. This term gives a tendency to align two spins vertically, and may cause the spin alignment of the material to deviate from simple ferromagnetic or antiferromagnetic order, resulting in rich noncollinear structures.[36,37] $H_{\rm Kitaev} = -K_\gamma \hat{S}_i^\gamma \hat{S}_j^\gamma$ ($\gamma = x$, y or z) is the Kitaev interaction Hamiltonian defined on honeycomb lattice, where $\hat{S}_i^\gamma$ and $\hat{S}_j^\gamma$ are the γ components of two spins at the edges of a bond, and γ depends on the spatial orientation of the bond. The sum is over all bonds.[38] The Kitaev spin model is a solvable model that supports quantum spin liquids (QSL) as its ground state, and has therefore been widely studied.[39–41]

In the case where the anisotropy A_α is not very strong, the above Eq. (1) is called the Heisenberg model. In the case of taking extreme high values of anisotropy, the Heisenberg model can be reduced to simpler models. For example, if the system has strong uniaxial anisotropy ($A_\alpha \to \infty$), then the system can be abstracted as an Ising model

$$\mathcal{H}_{{\rm Ising}.\alpha} = -\sum_{i<j} J_{ij} \hat{S}_{i\alpha} \hat{S}_{j\alpha}, \quad (\alpha = x, y \ \text{or} \ z). \tag{2}$$

The Ising model has the strongest anisotropy and therefore has a stable long-range order in two-dimensional situations. If the system has strong easy plane anisotropy ($A_z \to 0$), it can be abstracted as an XY model

$$\mathcal{H}_{XY} = -\sum_{i<j} J_{ij} \left(\hat{S}_{ix} \hat{S}_{jx} + \hat{S}_{iy} \hat{S}_{jy}\right). \tag{3}$$

The spins in the XY model can point in any direction in the xy plane, which means weaker anisotropy than the Ising model, and therefore there is no long-range order; but there is a quasilong-range order, and the phase transition associated with it is the Berezinskii–Kosterlitz–Thouless (BKT) phase transition.[42–44]

2.2. Magnons in 2D ferromagnetic Heisenberg model and Mermin–Wagner theorem

In this section, we take the 2D ferromagnetic Heisenberg model as an example to introduce the definition of a magnon and explain why anisotropy plays a crucial role in stabilizing 2D magnetic order. The simplest model only considers $\mathcal{H}_{\rm ex}$ and $\mathcal{H}_{\rm a}$. If there is no magnetic anisotropy at all, the behavior of the system is determined only by the complete exchange interaction $\mathcal{H}_{\rm ex}$. As an example of solving a magnon, we consider a square lattice, where each cell contains only one spin, there is only nearest neighbor exchange interaction, and all J_{ij} are equal and greater than 0 ($J_{ij} = J > 0$ for nearest neighbor; $J_{ij} = 0$ for other neighbor). Therefore, the Hamiltonian (1) can be simplified to

$$\begin{aligned} \mathcal{H}_{\rm FM} &= -\sum_{l,\delta} J \hat{\boldsymbol{S}}_l \cdot \hat{\boldsymbol{S}}_{l+\delta} \\ &= -\sum_{l,\delta} J \left(\hat{S}_{lx} \hat{S}_{l+\delta,x} + \hat{S}_{ly} \hat{S}_{l+\delta,y} + \hat{S}_{lz} \hat{S}_{l+\delta,z}\right), \end{aligned} \tag{4}$$

where $\boldsymbol{\delta}$ is lattice constant ($\boldsymbol{\delta} = a\hat{x}, a\hat{y}$). The sum of l is over all cells, and the sum of $\boldsymbol{\delta}$ is over all nearest spins. In linear spin wave theory (LSWT),[45] we assume that the spins have a stable ground state, in ferromagnetic situation, all along z axis ($\boldsymbol{S} = S\hat{z}$). The magnon is defined as the small fluctuation near the ground state. Then we use the Holstein–Primakoff (HP) transformation[46]

$$\begin{cases} \hat{S}_z = S - \hat{a}^\dagger \hat{a}, \\ \hat{S}_+ = \hat{S}_x + {\rm i}\hat{S}_y = \sqrt{2S - \hat{a}^\dagger \hat{a}}\,\hat{a} \approx \sqrt{2S}\hat{a}, \\ \hat{S}_- = \hat{S}_x - {\rm i}\hat{S}_y = \hat{a}^\dagger \sqrt{2S - \hat{a}^\dagger \hat{a}} \approx \hat{a}^\dagger \sqrt{2S}, \end{cases} \tag{5}$$

where $\hat{a}$ $\left(\hat{a}^\dagger\right)$ is boson annihilation (creation) operator. By substituting it back to the Hamiltonian (4) and omitting terms higher than quadratic, the transformed Hamiltonian is

$$\begin{aligned} \mathcal{H}_{\rm FM} &= -J\sum_{l,\delta} S^2 + 2JS\sum_{l,\delta} \hat{a}_l^\dagger \hat{a}_l \\ &\quad - JS\sum_{l,\delta} \left(\hat{a}_{l+\delta}^\dagger \hat{a}_l + \hat{a}_l^\dagger \hat{a}_{l+\delta} + \delta_{l,l+\delta}\right) \\ &= -NZJS^2 - NJS + 2JSZ\sum_l \hat{a}_l^\dagger \hat{a}_l \\ &\quad - JS\sum_{l,\delta} \left(\hat{a}_{l+\delta}^\dagger \hat{a}_l + \hat{a}_l^\dagger \hat{a}_{l+\delta}\right), \end{aligned} \tag{6}$$

where N is the number of cells, Z is the coordination number ($Z = 4$ for square lattice). By applying periodic boundary

conditions and performing a Fourier transformation, we obtain

$$\begin{cases} \hat{a}_l = N^{-\frac{1}{2}} \sum\limits_k \mathrm{e}^{\mathrm{i}k\cdot l} \hat{a}_k, \\ \hat{a}_l^\dagger = N^{-\frac{1}{2}} \sum\limits_k \mathrm{e}^{-\mathrm{i}k\cdot l} \hat{a}_k^\dagger. \end{cases} \tag{7}$$

We then have

$$\mathcal{H}_{\mathrm{FM}} = -NZJS^2 - NJS + \hbar\omega_k \sum_k \hat{a}_k^\dagger \hat{a}_k. \tag{8}$$

This constitutes a harmonic oscillator, which we identify as magnons. We call $\hat{a}$ $\left(\hat{a}^\dagger\right)$ the creation (annihilation) operator of magnons. The $\hbar\omega_k$ is the energy of magnons, which depends on the structure and magnetic interaction. In our assumption, it has a form like

$$\begin{aligned} \hbar\omega_k &= 2ZJS(1-\gamma_k) \\ &= 2ZJS\left(1 - \frac{1}{Z}\sum_{\boldsymbol{\delta}} \mathrm{e}^{\mathrm{i}\boldsymbol{k}\cdot\boldsymbol{\delta}}\right) \\ &= 2ZJS\left(1 - \frac{2}{Z}\left(\cos k_x a_1 + \cos k_y a_2\right)\right) \\ &= 2ZJS\left(1 - \frac{1}{2}\left(\cos k_x a + \cos k_y a\right)\right), \end{aligned} \tag{9}$$

where $\gamma_k = \frac{1}{Z}\sum_{\boldsymbol{\delta}} \mathrm{e}^{\mathrm{i}\boldsymbol{k}\cdot\boldsymbol{\delta}}$. For small $\boldsymbol{k}$, $\hbar\omega_k \approx 2JSa^2\boldsymbol{k}^2$, so the magnon is gapless, with a density of states (DOS) given by $g(\omega) = \frac{1}{4\pi JSa^2}$. Since magnons obey Bose–Einstein statistics, their occupation number diverges as the energy approaches zero. Therefore, any size of fluctuation will excite a large number of magnons, resulting in the absence of stable magnetic order in a 2D Heisenberg system. While in 3D magnetic Heisenberg system, $g(\omega) \sim \sqrt{\omega}$ with small $\boldsymbol{k}$,[10] which is low at zero energy, so even gapless, the magnons created by thermal fluctuation are not enough to break the magnet order. In 1966, a theory called Mermin–Wagner theorem[47] has pointed out that the enhanced spin fluctuations in the 2D limit necessarily destroy any long-range or quasi-long-range orders at finite temperature in 2D isotropic Heisenberg magnets. Then, how can we talk about magnons in vdW magnets?

In fact, this instability can be eliminated by introducing anisotropy. As an example, by introducing a uniaxial anisotropy $\mathcal{H}_{\mathrm{a}} = -\sum_l A_z \hat{S}_{lz}^2$ into Eq. (4) and repeating the derivation process above, we obtain

$$\hbar\omega_k = 4JS\left(1 - \frac{1}{2}\left(\cos k_x a_1 + \cos k_y a_2\right)\right) + SA_z, \tag{10}$$

where $\hbar\omega_k \neq 0$ at $\boldsymbol{k} = 0$. To make it more apparent, we can also calculate the density of states of the magnon as $g(\omega) = 0\,(\hbar\omega < SA_z)$, $\frac{1}{4\pi JSa^2}\,(\hbar\omega > SA_z)$. Obviously, the existence of anisotropy introduces energy gaps. Therefore, when the characteristic energy of thermal fluctuations $k_{\mathrm{B}}T$ (k_{B} is the Boltzmann constant) is insufficient to overcome the energy gap SA_z and excite a magnon, the 2D magnet system remains stable.

2.3. Magnons in 2D antiferromagnetic Heisenberg model

In the previous section, we used the 2D ferromagnetic Heisenberg model as an example to introduce the basic principles of the magnon. In this section, we continue to discuss the definition of magnon in AFM. The basic physical concepts are the same. The vdW AFM can be classified into the following different types. If antiferromagnetic interactions only exist in interlayer coupling, while intralayer coupling remains ferromagnetic interactions, this type of magnet is called A-type AFM. On the contrary, if antiferromagnetic interactions only exist in intralayer coupling, while interlayer coupling remains ferromagnetic, it is C-type AFM. If there is antiferromagnetic coupling both within and between layers, it is G-type AFM. For C-type AFM and G-type AFM with in-plane antiferromagnetic ordering, there are different types depending on the static magnetic structure, such as Néel AFM (nAFM), stripe AFM (sAFM), zigzag AFM (zAFM), etc.

We consider the simplest single-layer square lattice Néel AFM as an example. In this type of AFM, the ground state magnetic structure is composed of two sets of ferromagnetic sub-lattices that are opposite in direction and nested across each other (strictly speaking, the Néel state is not a true ground state by considering quantum fluctuations, but it is close enough to the real ground state that we usually consider it as the ground state without any problems). For simplicity, we only consider exchange interactions, so the Hamiltonian is

$$\mathcal{H}_{\mathrm{Neel}} = |J| \sum_{l,\delta} \left(\hat{\boldsymbol{S}}_{al} \cdot \hat{\boldsymbol{S}}_{a,l+\delta} + \hat{\boldsymbol{S}}_{bl} \cdot \hat{\boldsymbol{S}}_{b,l+\delta}\right). \tag{11}$$

We assume that the spin direction of sub-lattice a is oriented towards $+z$, while the spin direction of sub-lattice b is oriented towards $-z$. Using the HP transformation

$$\begin{cases} \hat{S}_{az} = S - \hat{a}^\dagger \hat{a}, \\ \hat{S}_{a+} = \sqrt{2S - \hat{a}^\dagger \hat{a}}\,\hat{a} \approx \sqrt{2S}\hat{a}, \\ \hat{S}_{a-} = \hat{a}^\dagger \sqrt{2S - \hat{a}^\dagger \hat{a}} \approx \hat{a}^\dagger \sqrt{2S}, \end{cases}$$
$$\begin{cases} \hat{S}_{bz} = \hat{b}^\dagger \hat{b} - S, \\ \hat{S}_{b+} = \hat{b}^\dagger \sqrt{2S - \hat{b}^\dagger \hat{b}} \approx \hat{b}^\dagger \sqrt{2S}, \\ \hat{S}_{b-} = \sqrt{2S - \hat{b}^\dagger \hat{b}}\,\hat{b} \approx \sqrt{2S}\hat{b}, \end{cases} \tag{12}$$

and the Fourier transform

$$\begin{cases} \hat{a}_l = N^{-\frac{1}{2}} \sum\limits_k \mathrm{e}^{\mathrm{i}k\cdot l} \hat{a}_k, \\ \hat{a}_l^\dagger = N^{-\frac{1}{2}} \sum\limits_k \mathrm{e}^{-\mathrm{i}k\cdot l} \hat{a}_k^\dagger, \end{cases}$$
$$\begin{cases} \hat{b}_l = N^{-\frac{1}{2}} \sum\limits_k \mathrm{e}^{-\mathrm{i}k\cdot l} \hat{b}_k, \\ \hat{b}_l^\dagger = N^{-\frac{1}{2}} \sum\limits_k \mathrm{e}^{\mathrm{i}k\cdot l} \hat{b}_k^\dagger, \end{cases} \tag{13}$$

we obtain

$$\begin{aligned} \mathcal{H}_{\mathrm{Neel}} &= -2NZS^2|J| + 2ZS|J| \sum_k \left(\hat{a}_k^\dagger \hat{a}_k + \hat{b}_k^\dagger \hat{b}_k\right) \\ &\quad + 2ZS|J| \sum_k \gamma_k \left(\hat{a}_k^\dagger \hat{b}_k^\dagger + \hat{a}_k \hat{b}_k\right), \end{aligned} \tag{14}$$

which exhibits interaction between two sub-lattices, so we should do diagonalization. The general method is to use the Bogoliubov transform[48]

$$\begin{pmatrix} \hat{\alpha}_k \\ \hat{\beta}_k^\dagger \end{pmatrix} = \begin{pmatrix} u_k & -v_k \\ -v_k & u_k \end{pmatrix} \begin{pmatrix} \hat{a}_k \\ \hat{b}_k^\dagger \end{pmatrix}, \tag{15}$$

where $\hat{\alpha}_k$ $(\hat{\alpha}_k^\dagger), \hat{\beta}_k$ $(\hat{\beta}_k^\dagger)$ satisfy the boson commutations, respectively. v_k and u_k are undetermined real numbers. This transformation aims to eliminate the cross term and obtain a diagonalized Hamiltonian

$$\mathcal{H}_{\text{Neel}} = E_0 + \sum_k \hbar\omega_k \left(\hat{\alpha}_k^\dagger \hat{\alpha}_k + \hat{\beta}_k^\dagger \hat{\beta}_k\right). \tag{16}$$

We obtain $u_k^2 = \frac{1}{2}(1+\Delta)$, $v_k^2 = -\frac{1}{2}(1-\Delta)$, $\Delta = 1/\sqrt{1-\gamma_k^2}$. The antiferromagnetic magnon energy is

$$\hbar\omega_k = 2ZS|J|\sqrt{1-\gamma_k^2}. \tag{17}$$

It can be inferred that each energy has two degenerate magnon bands, which correspond to two sublattices.

Following the approach applied to the ferromagnetic system, we introduce a uniaxial anisotropy term[49] $\mathcal{H}_{\text{a}} = -A_z \sum_l \left(\hat{S}_{a,lz}^2 + \hat{S}_{b,lz}^2\right)$ into Eq. (11). Through analogous derivation procedures corresponding to Eqs. (12)–(17), the modified dispersion relation becomes

$$\hbar\omega_k = \sqrt{\left(8|J|S\left(1+\frac{1}{2}(\cos k_x a + \cos k_y a)\right)+2SA_z\right)\left(8|J|S\left(1-\frac{1}{2}(\cos k_x a + \cos k_y a)\right)+2SA_z\right)}. \tag{18}$$

This dispersion reveals a characteristic gap $\Delta = \sqrt{(16|J|S+2SA_z)2SA_z}$ at $\boldsymbol{k}=0$. In contrast to the ferromagnetic case described by Eq. (10), where the gap depends solely on the anisotropy parameter SA_z, the antiferromagnetic gap exhibits dependence on both exchange interaction and anisotropy. Given that the exchange interaction energy typically dominates over the anisotropy energy in antiferromagnetic systems,[50] the resulting magnon frequencies in antiferromagnets are substantially higher than those observed in ferromagnetic materials.[51–56]

For more complex magnetic structures such as sAFM, zAFM, or nAFM, as well as more complex interactions, the solution approach is similar. Figure 1 lists magnon dispersion for some typical vdW magnets. It is worth noting that if there are more than one magnetic site in each cell, the bands can be divided into acoustic magnons and optical magnons. For instance, CrSBr, an A-type antiferromagnet with two magnetic sites per unit cell, exhibits non-degenerate magnon bands along both Γ–X and Y–Γ directions (Fig. 1(a)). CrI_3 — a honeycomb-lattice magnet also containing two magnetic sites per unit cell — displays a magnon dispersion relation analogous to graphene's electronic band structure (Fig. 1(b)). The kagome-lattice system, featuring three magnetic sites per unit cell, correspondingly shows three magnon bands (Fig. 1(d)).

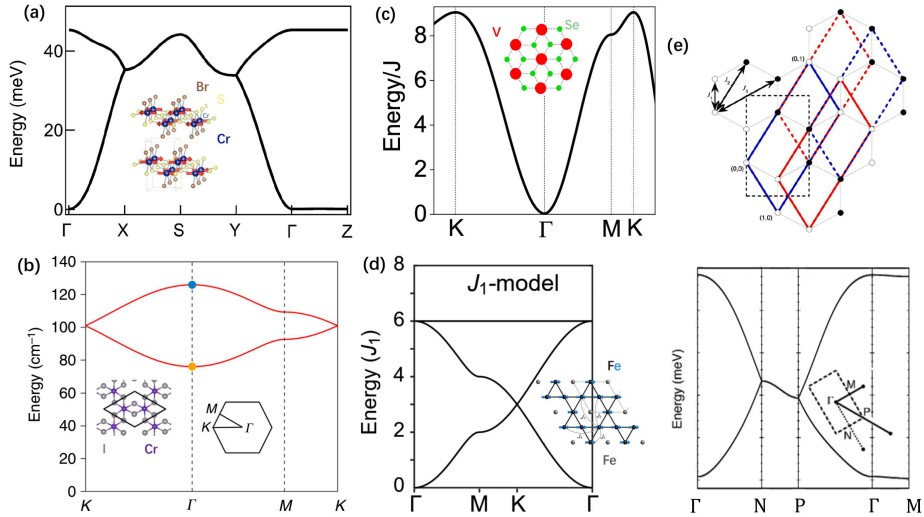


Fig. 1. Magnon dispersions for some typical vdW magnet structures. (a) Orthorhombic vdW magnet, e.g., CrSBr; (b) honeycomb vdW magnet, e.g., CrI_3; (c) hexagonal vdW magnet, e.g., VSe_2; (d) kagome vdW magnet, e.g., $Co_3Sn_2S_2$ or Nb_3Cl_8; (e) zigzag AFM, e.g., $FePS_3$. Figures are reproduced with permission from Refs. [57–62].

3. Magnons in vdW materials

Typical crystal structures of vdW magnets include orthorhombic crystal, honeycomb crystal, hexagonal crystal and kagome crystal, etc. We have summarized some important studies in Table 1. In this section, we will introduce some of the recent studies of magnons in these structures.

Table 1. Recent studies of magnons in vdW magnets.

	vdW magnets	Crystal structures	Specific materials and recent studies
3d transition metal halides	MX_3 ($MX_{3/2}$, M = V, Cr, Mn, Fe, Co, Ni; X = Cl, Br, I)	honeycomb	VI_3,[63,64] $CrCl_3$,[65–68] $CrBr_3$,[67,69–71] CrI_3,[67,72–76]
	MX_2 ($MX_{3/2}$, M = V, Cr, Mn, Fe, Co, Ni; X = Cl, Br, I)	hexagonal	$FeCl_2$,[77] CoI_2,[78] NiI_2,[79–82] $NiCl_2$/$NiBr_2$[82]
3d transition metal chalcogenides	1T-MX_2 (MX_2, M = V, Cr, Mn, Co; X = S, Se, Te)	hexagonal	
	2H-MX_2 (MX_2, M = V, Cr, Mn, Co; X = S, Se, Te)	hexagonal	
Ternary 3d transition metal compounds	CrXTe$_3$ (X = Si, Ge, Sn)	honeycomb	$CrSiTe_2$,[83] $CrGeTe_2$,[83,84]
	MPX_3 (MX_2, M = V, Cr, Mn, Fe, Co; X = S, Se, Te)	honeycomb	VPS_3,[85] $MnPS_3$,[86–91] $MnPSe_3$,[92–97] $FePS_3$,[98–108] $FePSe_3$,[109–111] $CoPS_3$,[112,113] $NiPS_3$[97,114,115]
	MXY (M = Ti, V, Cr, Fe; X = O, S, Se, Te; Y = Cl, Br, I)	orthorhombic	CrSBr,[57,58,116–121] $CrPS_4$,[122–126]
	Fe_nGeTe_2	honeycomb	
	$MnBi_nTe_m$	hexagonal	$MnBi_2Te_4$[122,127–129]
4d transition metal halides	α-RuX_3 (X = Cl, Br, I)	honeycomb	α-$RuCl_3$,[130–134] α-$RuBr_3$[135]
	Nb_3X_8 (X = Cl, Br, I)	kagome	

3.1. Orthorhombic crystal

The orthorhombic crystal structure is the simplest structure, while, to date, only the ternary 3d transition metal compounds (MXY, M = Cr, Fe; X = O, S, Se; Y = Cl, Br, I) have been found to satisfy the orthorhombic crystal structure among the known vdW magnets. In this family, the CrSBr,[57,58,116,118,120,121,136] an A-type AFM, is the material that has been most extensively studied. In each unit cell, there are two magnetic atoms, thus giving rise to two magnon branches. The magnon dispersion is shown in Fig. 1. The magnons in CrSBr have been discovered by many methods, such as inelastic neutron scattering for bulk,[58] microwave absorption spectroscopy (Fig. 2)[118,121] and time-resolved absorption spectroscopy[57,120] for few layers. Cham has detected the optical and acoustic magnon in CrSBr by antiferromagnetic resonances, and quantified the parameters governing the magnetic dynamics. Bae[57] has reported that due to the interlayer antiferromagnetic coupling, the Brillouin zone along c-axis fold into the half, as a result, the two magnon branches both split into two sub branches: in-phase and out-of-phase (which are not shown in Fig. 1). Another popular material in this family is $CrPS_4$,[123–125,137] which is also an A-type AFM. The $CrPS_4$ shows huge in-plane anisotropy, which causes anisotropic magnon transport.[126]

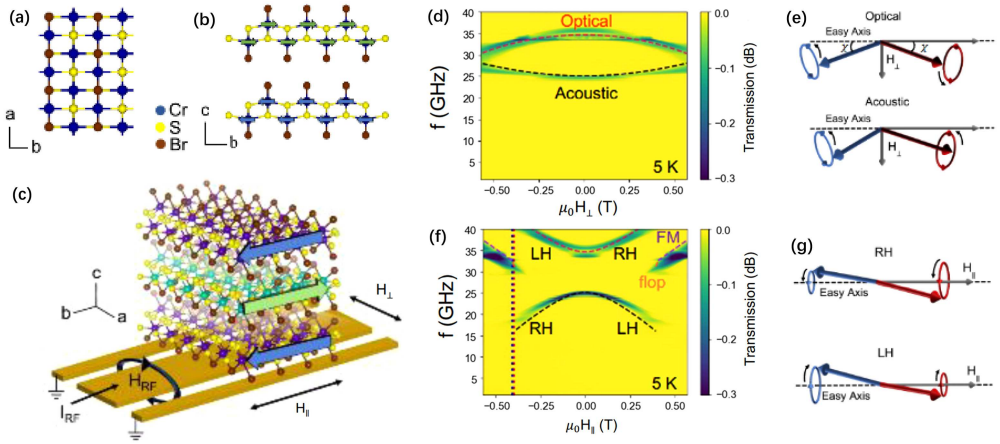


Fig. 2. Magnons in CrSBr detected by microwave absorption spectroscopy. (a)–(b) Crystal structure of CrSBr. (c) Experimental schematic of a CrSBr crystal mounted on a coplanar waveguide for microwave absorption measurements. The microwave magnetic fields are perpendicular to the magnetic a axis. External fields can be applied either parallel ($H_\parallel$) or perpendicular ($H_\perp$) to the a axis. (d)–(e) Microwave absorption spectra measured at 5 K as a function of magnetic field $H_\perp$. (f)–(g) Microwave absorption spectra measured at 5 K as a function of magnetic field $H_\parallel$. Reprinted with permission from Ref. [121], Copyright 2022 American Chemical Society.

3.2. Honeycomb crystal

Just like graphene and many other vdW materials, the honeycomb crystal structure encompasses many interesting physical properties. The main reason is that it exhibits linear dispersion at the corner of the Brillouin zone, specifically at the K and K' points in group theory, known as the Dirac cone, which supports massless excitations. A wide range of vdW magnets belongs to this family, including transition metal trihalides (MX_3), ternary transition metal compounds (CrXTe$_3$ and MPX_3) and Fe_nGeTe_2 ($3 \leq n \leq 5$), where we can find almost all kinds of magnet types we have introduced in Section 2. An extensively studied example is

CrI_3,[73–76,138,139] a FM with an easy axis along z-axis, in which the magnon dispersion with two Dirac cones is shown in Fig. 1(e). As a comparison, the materials with same metal elements, $CrCl_3$[65–68,72] and $CrBr_3$,[67,69–71] are easy-plane and isotropic, respectively. Their magnons are reported by inelastic neutron scattering[72,140] for bulk, Raman scattering,[73,75] microwave absorption spectroscopy,[74] inelastic magneto-tunneling spectroscopy[139] and time-resolved absorption spectroscopy[74] for few layers to monolayer, some results are shown in Fig. 3. Just as graphene does, honeycomb magnets carry Dirac magnons at the K and K' points of the Brillouin zone. Just like spin–orbit coupling, the DMI and the Kitaev interaction play the similar role in opening the Dirac cone and creating a band gap.[140,141]

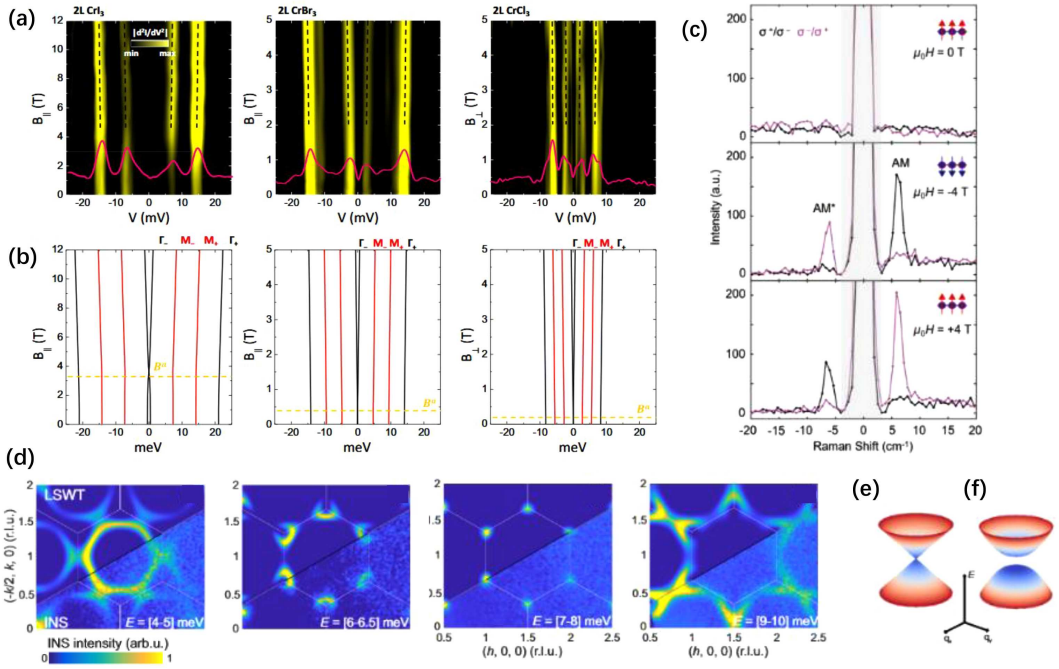


Fig. 3. Magnons in CrX_3. (a)–(b) Inelastic tunneling spectroscopy of magnons in 2L CrX_3. (a) Field-dependent d^2I/dV^2 vs. V for 2L CrX_3 at 0.3 K and (b) calculated magnon energies for 1L CrX_3 with magnetic field applied along the hard axis. Magnon peaks in (a) are partially guided by dashed lines. (c) Low-frequency cross-polarized Raman spectra taken at zero field, −4 T and 4 T. The grey box indicates the spectral range of the optical filter below which the magnon is unresolvable. (d) Inelastic neutron scattering intensity of $CrBr_3$ obtained by integrating the $E_i = 30$ meV dataset over four constant-energy windows (indicated) and compared with linear spin-wave theory (LSWT). (e)–(f) Schematic spin-wave spectra in the vicinity of the K points of $CrBr_3$. When inversion symmetry is preserved, $\omega_q \propto q$ and the dispersion forms a Dirac cone (e); otherwise, a gap opens to form separate acoustic and optical magnon branches (f). Figures (a)–(b), (c) and (d)–(f) are reproduced with permission from Refs. [73,139], and [69], respectively.

Expect for transition metal trihalides, the ternary transition metal compounds also include a large range of vdW magnets. There are ferromagnetic semiconductors $CrXTe_3$ (X = Si, Ge, Sn) and AFM MPX_3 (M = V, Cr, Mn, Fe, Co and Ni; X = S, Se, and Te). In the MPX_3 family, magnons have already been observed in Heisenberg AFM $MnPS_3$,[86–91] XY AFM $NiPS_3$,[15,16,97,114,115,142,143] $MnPSe_3$,[92–96] $CoPS_3$,[112,113] and Ising AFM $FePS_3$[98–108,144] and $FePSe_3$[109–111,145] Among these, $FePS_3$, $FePSe_3$, $NiPS_3$, and $CoPS_3$ have zigzag magnet order, while $MnPS_3$ and $MnPSe_3$ have Neel magnet order. What's more, the strong coupling between magnons and phonons has been observed in $FePS_3$,[101–103] $FePSe_3$[110] and $MnPSe_3$,[146] which is of great significance for the development of magnonic devices.

Fe_nGeTe_2 ($3 \leq n \leq 5$) is a kind of vdW magnet that can remain magnet order up to room temperature (220 K for Fe_3GeTe_2, 270 K for Fe_4GeTe_2 and 300 K for Fe_5GeTe_2).[147,148] The discovery of magnons in these materials will provide great benefits for the application of vdW magnets in magnonics, but there is still no direct experimental evidence.

3.3. Hexagonal crystal

Few experimental results about magnons have been reported in this structure, while it is an important structure that consists of many vdW families, such as transition metal dihalides (MX_2, M = V, Cr, Mn, Fe, Co; X = F, Cl, Br, I), transition metal dichalcogenides (MX_2, M = V, Cr, Mn, Co; X = S, Se, Te; H-phase and T-phase) and $MnBi_{2n}Te_{3n+1}$ ($n = 1, \ldots, 4$). One well studied material is $MnBi_2Te_4$, an intralayer ferromagnetic vdW magnet, which is predicted and experimentally shown to be axion insulator for odd layer[18] and quantum anomalous Hall insulator for even layer[17,19,149] because of its topological structure. The magnon of $MnBi_2Te_4$ has been found by inelastic neutron scattering,[150] time-resolved magneto-optical Kerr spectrum,[129] time-resolved reflection spectrum[129] and Raman spectrum.[127] In two-

septuple layer $MnBi_2Te_4$ with non-trivial topology, magnon characteristics evolve as an external magnetic field tunes the ground state through three ordered phases: antiferromagnet (AFM), canted antiferromagnet (c-AFM), and ferromagnet (FM), which include two magnon modes, respectively. Theoretically, only the modes with $\mathcal{ITC}$, $\mathcal{CT}$ and $\mathcal{I}$ symmetry ($\mathcal{I}$ represents inversion, $\mathcal{T}$ represents time-reversal; $\mathcal{C}$ represents rotation) are Raman active. While Lujan[127] found that the Zeeman shift in AFM disappears, in favor of a narrow two-magnon peak, which is shown in Fig. 5. For intralayer hexagonal AFM, there exists geometrical frustration, so that the magnet order can be noncollinear. Materials like $NiBr_2$[82] and NiI_2[79–82] belong to this group, while there are still no experimental results reporting magnons in them.

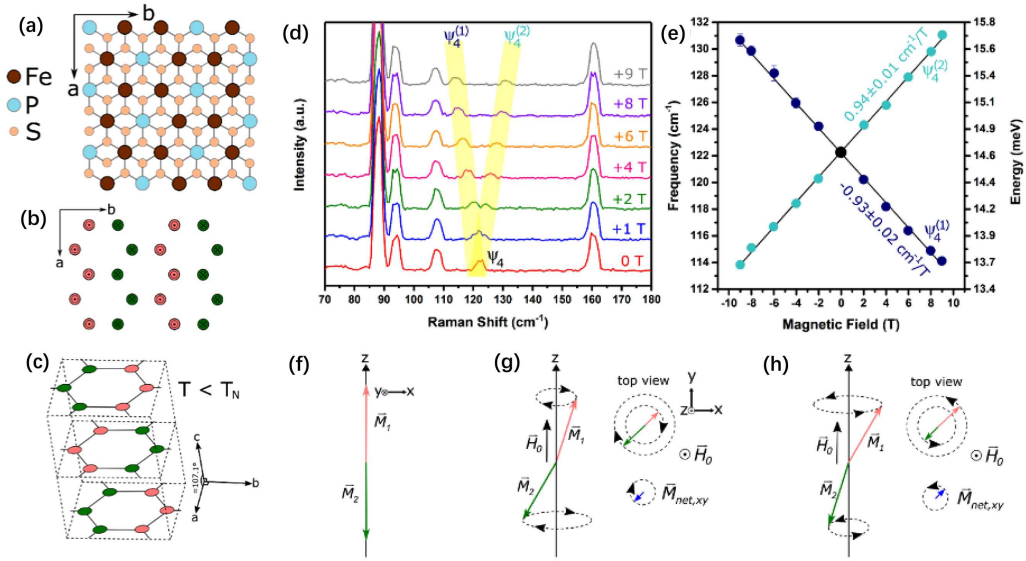


Fig. 4. Magnons in $FePS_3$. (a) Top view of $FePS_3$ crystal structure. (b) The zigzag antiferromagnetic magnetic structure of $FePS_3$ below the Néel temperature T_N. Only the Fe atoms in $FePS_3$ are shown, where spin up and spin down are labeled in pink and green, respectively, and the zigzag spin chains are arranged along the a-axis. (c) There is antiferromagnetic coupling between layers. (d) The Raman spectra of $FePS_3$ under magnetic field of 0–9 T at $T = 5$ K, indicating that under a finite magnetic field, the magnon splits into two branches, and its dispersion can be fitted as the linear dispersion shown in (e). (f)–(h) Diagram of antiferromagnetic magnon at Γ point. The two magnetization sub-lattices of AFM can be simplified as two macro-spins M_1 (pink) and M_2 (green). In the ground state M_1 and M_2 points are in the $+z$ and $-z$ directions, shown in (f), include two degenerate magnon modes. At finite magnetic field, the degeneracy of these modes is broken into $\psi_4^{(1)}$ and $\psi_4^{(2)}$, shown in (g) and (h), respectively. Figures (a)–(h) are adapted from Ref. [106].

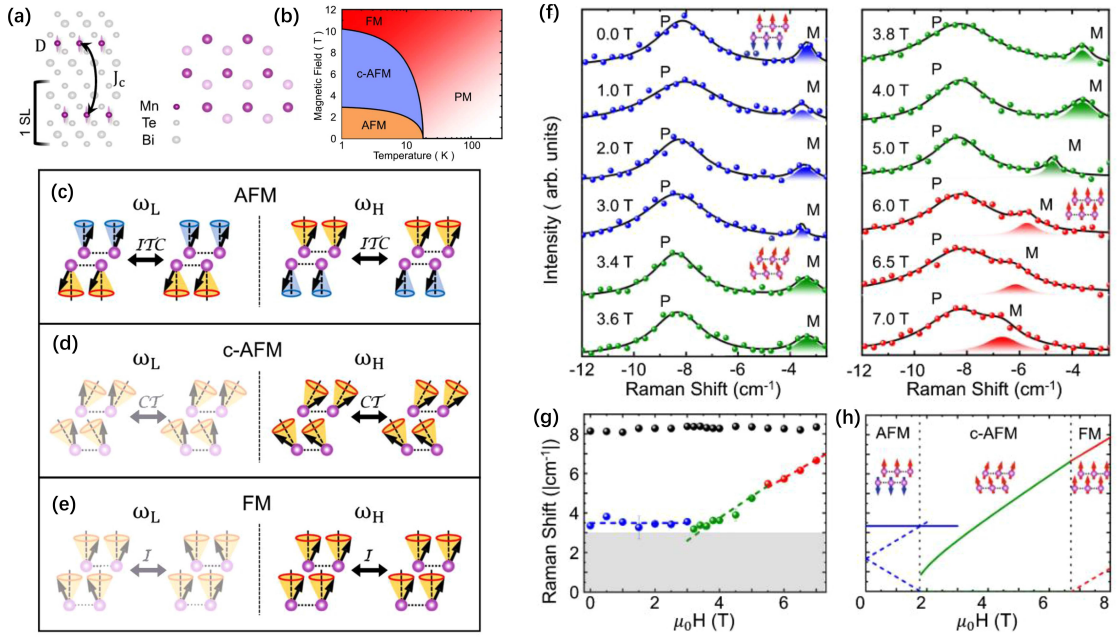


Fig. 5. Magnons in 2L $MnBi_2Te_4$. (a) Illustration of two triangular magnetic lattices formed by Mn ions in the top (bottom) layer indicated by dark (light) purple spheres. The layers follow an ABC stacking order. D and J_c represent anisotropy and interlayer exchange coupling. (b) Phase diagram as a function of temperature and an applied magnetic field perpendicular to the 2D plane. (c)–(e) Magnons in AFM, c-AFM and FM phases. Two modes in AFM unchanged after $\mathcal{ITC}$, one mode in c-AFM unchanged after $\mathcal{CT}$, and one mode in FM unchanged after $\mathcal{I}$, they are Raman active theoretically. (f) Raman spectra at 12 K as a function of magnetic field. P and M represent phonon and magnon, respectively. (g) Extracted central frequency for both the phonon and magnon vs. magnetic field. (h) Calculated magnon modes in the AFM, c-AFM and FM phases. Figures (a)–(h) are reproduced with permission from Ref. [127].

3.4. Kagome crystal

Kagome crystal structure is similar to honeycomb crystal, while there are three magnet atoms in each unit cell. Among the three bands, one of them is flat, the others are similar to the two bands in honeycomb crystal. In the flat band, the magnet energy is the same in the whole Brillouin zone, which means the kinetic energy of magnons is cancelled out, and the magnons are localized. A possible material family is Nb_3X_8 (X = Cl, Br and I),[151,152] where Nb forms breathing kagome crystal. However, some experiments show that they actually are Mott insulators, and the magnetism comes from the Nb_3 trimers, which form a hexagonal lattice.[153] Another important reason why the kagome crystal has attracted attention is that its ground state is believed to potentially be quantum spin liquid (QSL), whose quasiparticle excitations are no longer magnons but spin-1/2 spinons.[154]

4. Experimental methods to detect magnons in vdW magnets

There are many methods for studying magnons in vdW magnets, such as inelastic neutron scattering, optical inelastic scattering, time-resolved spectroscopy, inelastic magneto-tunneling spectroscopy, etc. Among them, inelastic neutron scattering can study the dispersion of magnons throughout the Brillouin zone, but it is only applicable to bulk samples. Optical methods can be used to study monolayer samples, but typically only the magnons at the center of the Brillouin zone can be detected. As a supplement to optical methods, transport methods can be used to study the magnons at the points with finite momentum of the Brillouin zone.

4.1. Inelastic neutron scattering

Inelastic neutron scattering is a commonly used technique for studying magnons in materials.[39,58,69,70,140,155–157] Neutrons are uncharged but with spin 1/2, which makes them suitable for investigating the magnetic properties of materials. Inelastic neutron scattering can be employed to study the dispersion and behavior of magnons through the energy exchange between neutrons and magnons in the material. Compared to optical methods, neutron scattering can provide the information about the dispersion of magnons across the entire Brillouin zone due to the large momentum of neutrons, as exemplified in Fig. 3. However, for vdW materials with micron-level dimensions and nano-level thickness layers, the signal from neutron scattering may be weak, making it challenging to use neutron scattering for studying these materials.[1] When it comes to the behavior of vdW magnets in the two-dimensional limit, neutron scattering is not an ideal method.

4.2. Optical methods

4.2.1. Raman spectroscopy

Raman spectroscopy is a convenient and non-destructive tool to characterize the quasiparticles in vdW materials.[2,158–162] The prominent features of Raman peaks, including frequency, full width at half maximum (FWHM), intensity and line shape, contain useful information to investigate the fundamental physical properties of 2D materials. The theory of magnon Raman spectroscopy was described by Fleury and Loudon in 1968.[163] According to their theory, light can interact with spins in two ways: by direct coupling between the magnetic field of the light and the spins and by indirect coupling, which means the light first couples to the electric dipole of the magnetic ions, then influences the spins through spin–orbit coupling. In Raman spectroscopy, the latter plays a more important role.

The Raman process satisfies the law of energy/momentum conservation, $\hbar\omega_{S(AS)} = \hbar\omega_i \mp \hbar\Omega$, $\boldsymbol{k}_{S(AS)} = \boldsymbol{k}_i \mp \boldsymbol{q}$, where $\hbar\omega_i/\boldsymbol{k}_i$ is the energy/momentum of the incident photons, $\hbar\Omega/\boldsymbol{q}$ is the energy/momentum of the quasiparticles and $\hbar\omega_{S(AS)}/\boldsymbol{k}_{S(AS)}$ is the energy/momentum of the Stokes/anti-Stokes photons. Because the momentum of light is very small ($\boldsymbol{k}_i, \boldsymbol{k}_{S(AS)} \sim 0$), the single quasiparticle Raman spectroscopy can only probe the information around the Γ point in the Brillouin zone. For the two-magnon process, all magnon pairs satisfying $\boldsymbol{k}_1 = -\boldsymbol{k}_2$ can be detected, while the pair on the boundary is the main component, reflecting the information of magnetic exchange coupling and spin fluctuations.[1] For example, the one-magnon scattering in $FePS_3$[106] and $MnPS_3$,[91] together with the two-magnon scattering in $NiPS_3$[14] have been revealed by Raman.

4.2.2. Brillouin spectroscopy

Like Raman spectroscopy, the Brillouin spectroscopy is also an inelastic light-scattering technique, which can detect lower energy quasiparticles than Raman.[164–167] Modern low-wavenumber Raman (LWNR) instruments utilize novel notch filters and fine gratings, which allow the detection of quasiparticles with minimum energies of ~150 GHz (~ 5 cm^{-1}) or higher. The Brillouin instruments use multi-pass tandem FP interferometer, so can probe quasiparticles with much lower energies in the range of 300 MHz to 900 GHz.[168] Usually the magnons have low energy, so the Brillouin spectroscopy is an effective method to study them.

4.2.3. Time-resolved optical spectroscopy

Optical spectroscopy like magnetic circular dichroism (MCD),[169,170] magneto-optical Kerr effect (MOKE),[171] magnetic linear dichroism (MLD),[172,173] etc., can get the magnetic information from materials. Furthermore, their time-resolved version can detect the coherent excitations, for exam-

ple, magnons. As in Fig. 6, Shi[134] used time-domain terahertz spectroscopy to measure the low energy conductivity and magnons in $RuCl_3$ under an external magnetic field. They have found a magnon with 0.62 THz at zero field below T_N, which is not affected by the external magnetic field H_{DC} along the c-axis, but is clearly suppressed when H_{DC} is applied within *ab* plane. When the magnetic component of THz wave $h(t)$ is perpendicular to the applied in-plane magnetic field, there is another coherent oscillation at slightly higher energy scale at the field above 2 T, which is eventually suppressed for $H_{DC} > 5$ T. The measurement indicates that the in-plane magnetic field can lift the degeneracy of two branches of low energy magnons at Γ point. Zhang[74] used ultrafast optical pump/magneto-optical Kerr probe technique to excite spin waves and probe their dynamics in AFM CrI_3 bilayers. What's more, some vdW magnets have strong magnon–exciton coupling, such as CrSBr, so that the time-resolved absorption spectra can indirectly reflect their magnon dynamics.[57,142]

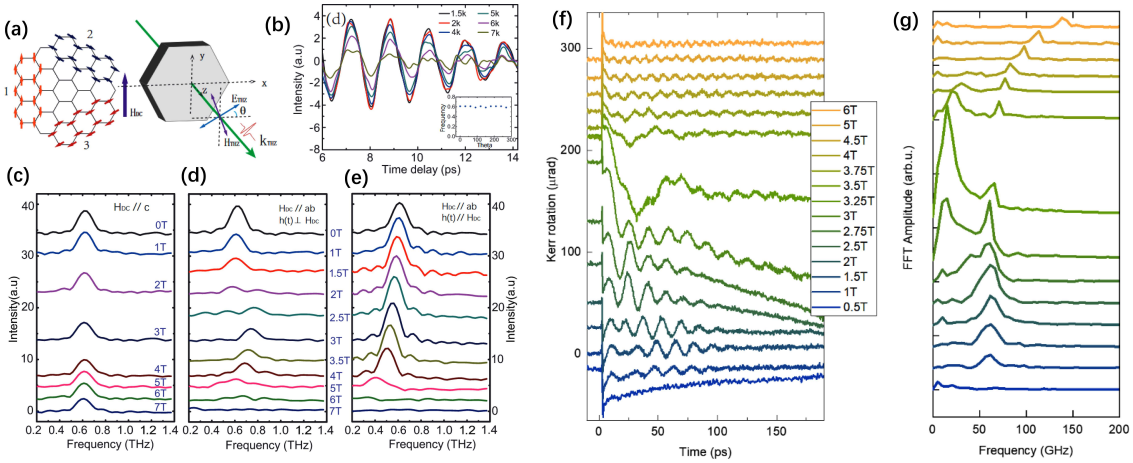


Fig. 6. Time-resolved optical spectroscopy is used to study magnons in α-$RuCl_3$ and CrI_3. (a) Schematic of three domain orientations of α-$RuCl_3$ with zigzag magnetic order and terahertz measurement. (b) Coherent magnon excitation of α-$RuCl_3$ in time domain at selected temperatures. The inset shows angle dependence of magnon excitation at 4 K. (c)–(e) Fourier transform of coherent magnon excitation of α-$RuCl_3$ in time domain at selected magnetic fields. (c) $H_{DC} \parallel c$ axis; (d) $H_{DC} \parallel ab$ plane and $H_{DC} \perp h(t)$; (e) $H_{DC} \parallel ab$ plane and $H_{DC} \parallel h(t)$. (f) Time-resolved magnon oscillations of bilayer CrI_3 detected by pump-induced Kerr rotation as a function of pump–probe delay time under different in-plane magnetic fields. (g) Fourier transform of (f). Figures (a)–(e) and (f)–(g) are reproduced with permission from Refs. [134] and [74], respectively.

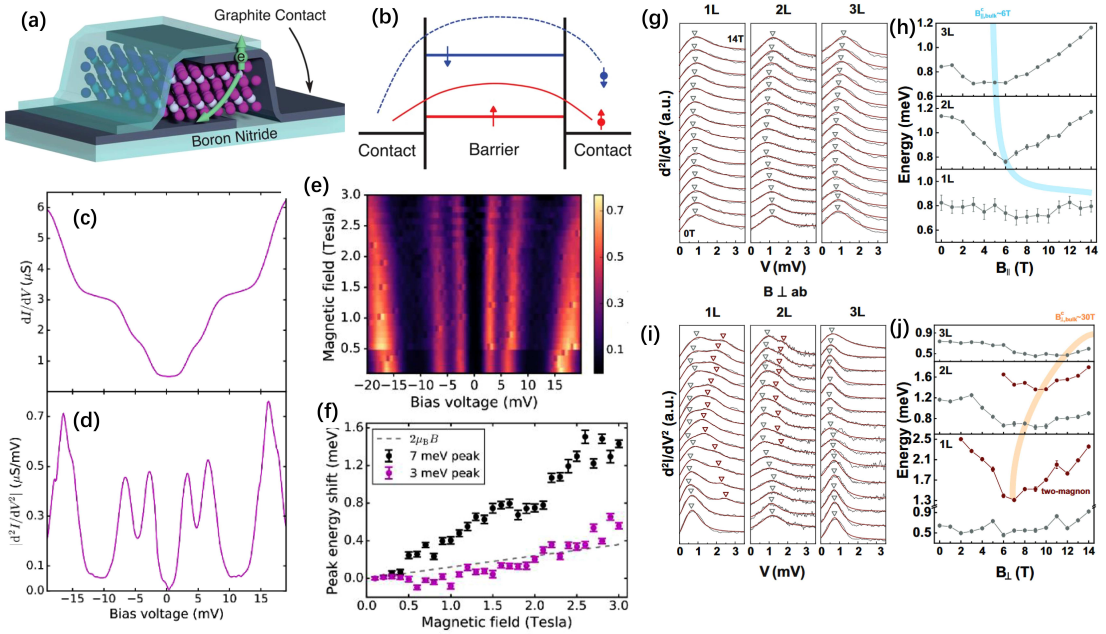


Fig. 7. Magnons in CrI_3 and α-$RuCl_3$ detected by inelastic magneto-tunneling spectroscopy. (a) Schematic of the CrI_3 tunnel junction device for inelastic magneto-tunneling spectroscopy. (b) Schematic energy diagram of a metal/ferromagnetic insulator/metal junction. The red and blue lines in the barrier region represent the spin-up and spin-down energy barriers, respectively. The lower barrier for spin-up electrons leads to spin polarized tunneling and reduced resistance for a ferromagnetic barrier. (c) dI/dV vs. DC bias voltage for a bilayer CrI_3 barrier device at zero applied magnetic field. (d) d^2I/dV^2 vs. DC bias voltage. According to the theory of inelastic tunneling spectroscopy, the peaks in (d) correspond to phonon or magnon excitations of the barrier or electrodes. (e) $|d^2I/dV^2|$ versus applied magnetic field and DC bias voltage. All three inelastic peaks increase in energy as the applied field is increased. (f) Energy of the two lowest energy inelastic peaks versus applied magnetic field. (g)–(j) shows the similar research of α-$RuCl_3$. (g) d^2I/dV^2 vs. DC bias voltage at different magnetic field $B \parallel ab$ plane, and the magnons energy is shown in (h); (i) and (j) are the same result when $B \perp ab$ plane. Figures (a)–(f) and (g)–(j) are reproduced with permission from Refs. [76,130], respectively.

4.3. Inelastic magneto-tunneling spectroscopy

Inelastic magneto-tunneling spectroscopy uses a magnet semiconductor as a barrier to detect the tunneling differential conductance $(\mathrm{d}I/\mathrm{d}V)$. If there is any inelastic scattering between the electron and other quasiparticles, then the density of states of the electron will change, and the $\mathrm{d}I/\mathrm{d}V$ will exhibit different signals. There are already some works that use this method to detect magnons in vdW magnets, such as CrX_3 (X = Cl, Br and I)[67,76] and α-$RuCl_3$.[130] Compared with optical methods, the inelastic magneto-tunneling spectroscopy can detect the magnons at finite momentum points, while the latter can only study the magnons at Γ point. For example, as shown in Figs. 7(a)–7(f), Kleih[76] detected the magnons at M point (the van Hove singularity point with a divergent magnon density of states).

5. Interaction between magnons and other quasiparticles

5.1. Phonons

The interaction between magnons and phonons creates hybridization between magnetic and phononic resonances, which provides methods to excite, manipulate, and detect magnons. The antiferromagnetic magnon has a frequency similar to optical phonons in the THz range, enhancing the coupling strength. In application, due to the typically large exchange interaction and the absence of dipolar fields, antiferromagnetic magnons can process information at a speed three orders of magnitude faster than FM magnons,[51–56] and they are more stable under small electromagnetic disturbances.[52,174] Based on the reasons above, the coupling between magnons and phonons in vdW AFM is becoming an emerging field. As shown in Fig. 8, Liu,[175] Vaclavkova[102] and Sun[101] *et al.* directly observed the strong coupling between magnons and phonons in $FePS_3$ by Raman spectroscopy. The magnon mode couples to the nearest phonon mode, and forms a magnon polaron pair, whose energy dispersion shows an anti-crossing character. In addition, the circular polarized Raman spectra show that the magnon transfers its spin to the phonon through the strong coupling under the out-of-plane magnetic field. Mai[176] has reported the hybridization of two-magnon continuum with two phonons in $MnPSe_3$, which can be described by a Fano-like model.

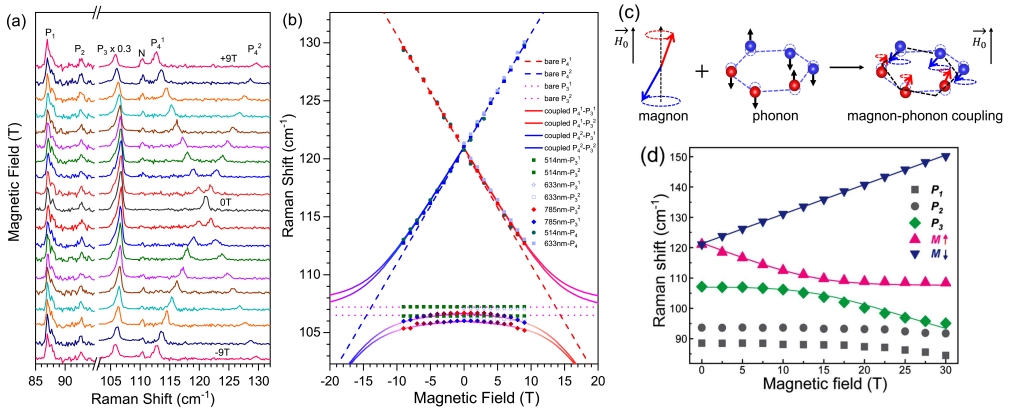


Fig. 8. The magnon–phonon coupling in $FePS_3$. (a) The Raman spectrum of phonons and magnons of $FePS_3$, and (b), (d) the magnon and phonon energies, include anti-crossing. (c) The Schematic diagram of magnon–phonon coupling. Reprinted with permission from Refs. [101, 175], Copyright 2022 American Chemical Society.

5.2. Excitons

Some vdW magnets are semiconductors, which feature both tightly-bound excitons with large oscillator strength and potentially long-lived coherent magnons due to the presence of bandgap and spatial confinement. While magnons and excitons are energetically mismatched by orders of magnitude, their coupling can lead to efficient optical access to spin information. Such 2D magnon–exciton coupling allows the launch and detection of spin waves from strong absorption, emission, or reflection of light in the energy range corresponding to excitonic transitions. An example is CrSBr, a A-type AFM with an excitonic gap 1.34 eV. The energy change of exciton $\Delta E_{\mathrm{ex}} \propto \cos^2 \frac{\theta}{2}$, where θ is the angle between the magnet moments between neighboring layers. As shown in Fig. 9, through this way, Bae[57] shows that the coherent magnons can be detected by time-resolved exciton sensing. Diederich[142] uses this method to show that by controlling the direction of applied magnetic fields relative to the crystal axes, the exciton can couple to not only the bright magnon, but also to an optically dark mode via magnon hybridization.

5.3. Magnon devices based on vdW magnets

The implementation of van der Waals (vdW) magnets in magnonic devices has emerged as a significant research frontier. Fundamental magnonic operations — including magnon generation, propagation, and detection — have been successfully established in vdW magnetic systems through experimental verifications.[177,178] Furthermore, the development of magnon-based computing architectures necessitates the implementation of nonlinear signal processing elements,

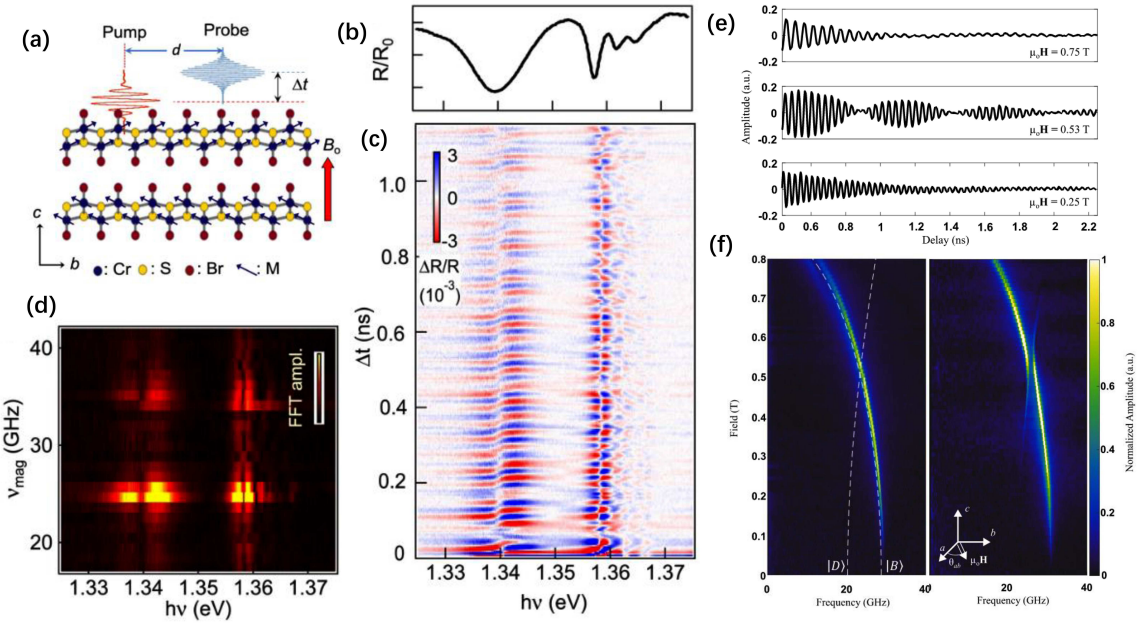


Fig. 9. Coupling of magnons and excitons in CrSBr. (a) The experiment configuration of transient reflectance. A femtosecond pump pulse with above gap photon energy launches spin waves in the layered AFM semiconductor CrSBr. Reflectance from a broadband probe pulse measures coherent oscillation at excitonic transitions. An external canting field, $B = 0.2$ T, is applied along the c-axis (normal to the 2D planes) to enhance the oscillatory signal. (b) Normalized reflectance of CrSBr. (c) Transient reflectance spectra $\Delta R/R$ as a function of pump–probe delay (Δt) and probe photon energy $(h\nu)$. (d) Fourier transform of Δt in panel (c), shows the two magnons at 24 GHz and 34 GHz. (e)–(f) Coherent coupling between the bright and dark magnon modes. (e) The transient optical reflectivity at selected magnetic field in time-domain, the beating at 0.53 T is attributed to the magnon hybridization, the magnetic field applied at $\theta_{ab} = 2^\circ$ to the a-axis. (f) The data in frequency domain, the first figure shows the situation that the magnetic field is along the a axis, while the second has the same magnetic field as (e). Inset shows the definition of θ_{ab}. The observed avoided crossing demonstrates the coherent hybridization between the bright and dark magnon branches. Figures (a)–(d) and (e)–(f) are reproduced with permission from Refs. [57,142], respectively.

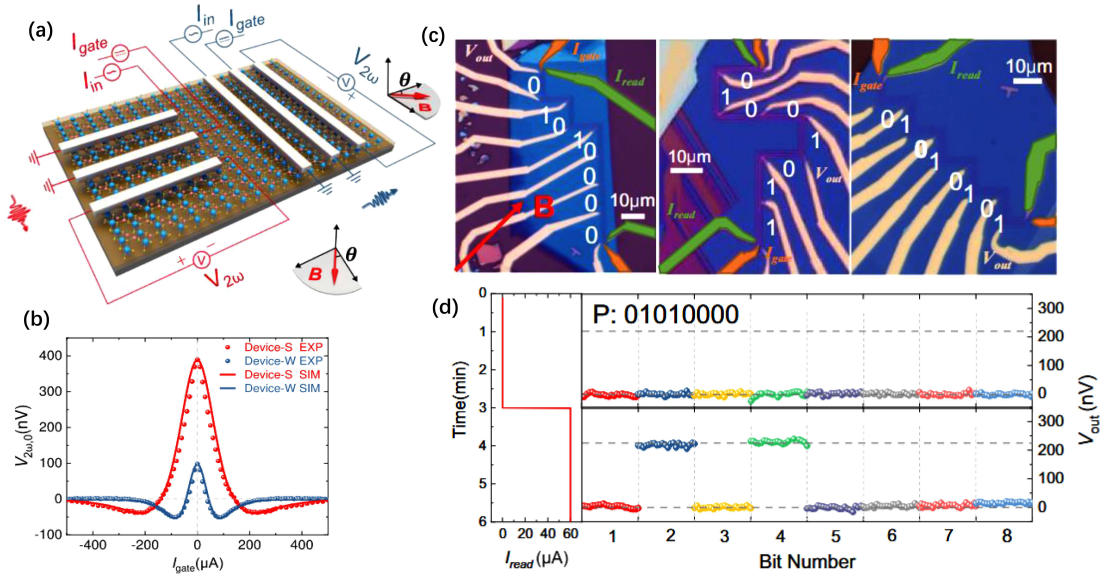


Fig. 10. The vdW magnon valve device and anisotropic magnon read-only memory (ROM). (a) Artistic schematics of the anisotropic magnon valve devices. Specifically, $I_{\rm in}$: AC injection current; $I_{\rm gate}$: DC gate current; $V_{2\omega}$: the second harmonic thermal magnon inverse spin Hall signal; θ: the angle of the in-plane magnetic field with respect to the direction perpendicular to the Pt electrodes. (b) Experimental and simulated $V_{2\omega,\theta=0}$ vs. $I_{\rm gate}$ curves at $B = 4$ T, $I_{\rm in} = 60$ μA and $T = 2$ K. Red and blue points show magnon transport signals taken along the ⟨010⟩ (device-S) and ⟨100⟩ (device-W) directions of the $CrPS_4$ crystal, respectively. Red and blue solid curves are respective simulations for device-S and device-W. (c) Three magnon ROM unit recording the letter "PKU" in ASCII codes. (d) Operation of the magnon ROM "P" with $I_{\rm read} = 0$ μA (not reading) and 60 μA (reading), respectively. When in the reading state, each magnon ROM unit generates an 8-bit series that represents a capital letter according to the ASCII codes.

analogous to transistor-based logic gates in conventional electronics. Such devices have been demonstrated by Chen[179] to be achievable through gated magnetic second-harmonic generation in $MnPS_3$, where thermal magnons are generated by an alternating current signal, then a second-harmonic signal is produced in the detection electrode via the inverse spin Hall effect. Arising from the nonlinear gate dependence of the non-equilibrium magnon density in the 2D spin chan-

nel, this second-harmonic signal can be modulated by a direct current gate current until it completely vanishes, thereby enabling logic gate operations, named vdW magnon valves. As shown in Fig. 10, using $CrPS_4$, experiments revealed that this effect can also depend on the propagation direction of the magnons[180] — specifically, the magnitude of the second-harmonic magnon signal differs in two mutually perpendicular crystal axes, which is related to the anisotropic spin Seebeck coefficient tensor of $CrPS_4$. Leveraging this property, a magnon-based memory device has been fabricated, where logic 0 and logic 1 are defined by the propagation direction of magnons in the waveguide. When magnons are excited, the stored information can be read out based on the value of the second-harmonic signal. While these developments highlight the potential of vdW magnets in magnonics, systematic integration of conventional magnonic device architectures with vdW material platforms remains essential for fully exploiting their unique advantages.

6. Conclusion and perspectives

In conclusion, we systematically summarize the core progress in the field of magnetic oscillator theory and experiments: at the theoretical level, we introduced the basic theory of ferromagnetic/antiferromagnetic magnons and its relation with Mermin–Wagner theorem, particularly highlighting its crucial implications for two-dimensional systems where thermal fluctuations play a dominant role. We clarify how this theorem governs the stabilization of 2D magnetic order through anisotropy, reconciling the theory-experiment discrepancy in low-dimensional systems.

At the experimental level, we summarize the magnons found in materials with different magnetic structures. We introduce the basic experimental technologies, including inelastic neutron scattering, Raman/Brillouin spectroscopy, time-resolved spectroscopy, and inelastic magneto-tunneling spectroscopy. In addition, we discuss the coupling between magnons and phonons/excitons, which can be used to clarify the properties of vdW magnets and provides new ideas for low-power spin information transmission and energy conversion.

In magnets, solitons such as domain walls, vortices and skyrmions that exist in equilibrium can be topologically protected.[181,182] There also exist solitons that act as robust excited states, such as spin wave bullet and spin wave droplets,[183] in which nonlinear interactions compensate the wave packet dispersion.[184] This kind of magnet soliton has been studied in thin magnetic films.[185,186] Van der Waals magnets or artificial magnonic lattices with topologically non-trivial structures may contain topologically nontrivial magnonic solitons, which are strongly influenced by the topological phase of the underlying lattice and will exhibit properties such as unidirectionally propagating edge states[187] and robust topological dynamic distinction.[184] Thus, it can be used for information storage and transfer. In recent years, the altermagnet has received widespread attention. The magnons in altermagnet have both linear and nondegenerate magnon dispersion compared with FM and AFM.[188,189] Many possible 2D altermagnets have been theoretically predicted,[188] and we expect the discovery and control of magnons within these systems. What's more, some vdW magnets don not have magnet order in their monolayers due to the quantum and thermal fluctuations, such as $NiPS_3$, a material that satisfies the 2D XXZ model, at low temperatures it behaves like a 2D XY model. It is believed that nontrivial magnetic excitations, such as Majorana particles,[190] spinons,[191] etc., can exist in these quantum-fluctuation-dominated systems. In addition, twist bilayer has been widely researched,[192] while the study of twist magnets just began a short time ago. Twisted vdW magnets may have moiré magnons,[24] topological magnons[193] and one-dimensional magnon network.[194] In addition, materials with stable magnetic order at room temperature are of great significance for the application of spin waves, such as Fe_nGeTe_2, we look forward to the research on the detection and manipulation of magnons in them.

For experimental methods, the optical method can only study the magnons at Γ point, while it is useful to access the full magnon dispersion in the full Brillouin zone momenta. However, it is challenging to use inelastic neutron scattering or non-resonant x-ray scatterings on micron-sized samples prepared via mechanical exfoliation due to the weak signal intensity. The resonant inelastic x-ray scatterings are needed to achieve sufficient signal-to-noise levels in few-layer samples.[195] In addition, the quantum sensors based on spin defects in solids can be used to image magnon transportation.[196–200] The nitrogen-vacancy (NV) centers in diamond can detect magnons via resonant coupling between the magnon frequency and the NV spin transitions, where magnon-induced fields drive coherent spin-state oscillations, measurable through optically detected magnetic resonance (ODMR).[200] ODMR has already been used to detect magnons in thin magnetic films made by bulk magnetic materials, such as YIG and $Ni_{80}Fe_{20}$.[197,198] We believe that its application in two-dimensional magnetic materials will bring new opportunities for studying magnon propagation, interference, and scattering with nanoscale resolution.[196,201]

Acknowledgements

J. Z. acknowledges the funding support from the Chinese Academy of Sciences — the Scientific and the CAS Project for Young Scientists in Basic Research (Grant No. YSBR-120) and the National Science Foundation of China (Grant No. NSFC12525405).

References

[1] Ahn Y, Guo X, Son S, Sun Z and Zhao L 2024 *Prog. Quantum Electron.* **93** 100498
[2] Sun Y J, Pang S M and Zhang J 2021 *Chin. Phys. B* **30** 117104
[3] Rahman S, Torres J F, Khan A R and Lu Y 2021 *ACS Nano* **15** 17175
[4] Zhang S, Xu R, Luo N and Zou X 2021 *Nanoscale* **13** 1398
[5] Mak K F, Shan J and Ralph D C 2019 *Nat. Rev. Phys.* **1** 646
[6] Gibertini M, Koperski M, Morpurgo A F and Novoselov K S 2019 *Nat. Nanotechnol.* **14** 408
[7] Gong C and Zhang X 2019 *Science* **363** eaav4450
[8] Wang X, Du K, Fredrik Liu Y Y, Hu P, Zhang J, Zhang Q, Owen M H S, Lu X, Gan C K, Sengupta P, Kloc C and Xiong Q 2016 *2D Mater.* **3** 031009
[9] Huang B, Clark G, Navarro-Moratalla E, Klein D R, Cheng R, Seyler K L, Zhong D, Schmidgall E, McGuire M A, Cobden D H, Yao W, Xiao D, Jarillo-Herrero P and Xu X 2017 *Nature* **546** 270
[10] Gong C, Li L, Li Z, Ji H, Stern A, Xia Y, Cao T, Bao W, Wang C, Wang Y, Qiu Z Q, Cava R J, Louie S G, Xia J and Zhang X 2017 *Nature* **546** 265
[11] Cenker J, Sivakumar S, Xie K, Miller A, Thijssen P, Liu Z, Dismukes A, Fonseca J, Anderson E, Zhu X, Roy X, Xiao D, Chu J H, Cao T and Xu X 2022 *Nat. Nanotechnol.* **17** 256
[12] Wilson N P, Lee K, Cenker J, Xie K, Dismukes A H, Telford E J, Fonseca J, Sivakumar S, Dean C, Cao T, Roy X, Xu X and Zhu X 2021 *Nat. Mater.* **20** 1657
[13] Lee K, Dismukes A H, Telford E J, Wiscons R A, Wang J, Xu X, Nuckolls C, Dean C R, Roy X and Zhu X 2021 *Nano Lett.* **21** 3511
[14] Kim K, Lim S Y, Lee J U, Lee S, Kim T Y, Park K, Jeon G S, Park C H, Park J G and Cheong H 2019 *Nat. Commun.* **10** 345
[15] Wildes A R, Stewart J R, Le M D, Ewings R A, Rule K C, Deng G and Anand K 2022 *Phys. Rev. B* **106** 174422
[16] Scheie A, Park P, Villanova J W, Granroth G E, Sarkis C L, Zhang H, Stone M B, Park J G, Okamoto S, Berlijn T and Tennant D A 2023 *Phys. Rev. B* **108** 104402
[17] Li J, Li Y, Du S, Wang Z, Gu B L, Zhang S C, He K, Duan W and Xu Y 2019 *Sci. Adv.* **5** eaaw5685
[18] Liu C, Wang Y, Li H, Wu Y, Li Y, Li J, He K, Xu Y, Zhang J and Wang Y 2020 *Nat. Mater.* **19** 522
[19] Gao A, Liu Y F, Hu C, *et al.* 2021 *Nature* **595** 521
[20] Cheng R, Okamoto S and Xiao D 2016 *Phys. Rev. Lett.* **117** 217202
[21] Nakata K, Kim S K, Klinovaja J and Loss D 2017 *Phys. Rev. B* **96** 224414
[22] Zhu H, Shi H, Tang Z and Tang B 2024 *Chin. Phys. B* **33** 037503
[23] Su Y, Wang X S and Wang X R 2017 *Phys. Rev. B* **95** 224403
[24] Li Y H and Cheng R 2020 *Phys. Rev. B* **102** 094404
[25] Hidalgo-Sacoto R, Gonzalez R I, Vogel E E, Allende S, Mella J D, Cardenas C, Troncoso R E and Munoz F 2020 *Phys. Rev. B* **101** 205425
[26] Van Kranendonk J and Van Vleck J H 1958 *Rev. Mod. Phys.* **30** 1
[27] Herring C and Kittel C 1951 *Phys. Rev.* **81** 869
[28] Bloch F 1930 *Z. Für Phys.* **61** 206
[29] Chumak A V, Vasyuchka V I, Serga A A and Hillebrands B 2015 *Nat. Phys.* **11** 453
[30] Zhang Z, Gao F Y, Chien Y C, Liu Z J, Curtis J B, Sung E R, Ma X, Ren W, Cao S, Narang P, Hoegen A von, Baldini E and Nelson K A 2024 *Nat. Phys.* **20** 788
[31] Huang C, Luo L, Mootz M, Shang J, Man P, Su L, Perakis I E, Yao Y X, Wu A and Wang J 2024 *Nat. Commun.* **15** 3214
[32] Serga A A, Chumak A V and Hillebrands B 2010 *J. Phys. Appl Phys.* **43** 264002
[33] Chumak A V, Serga A A and Hillebrands B 2014 *Nat. Commun.* **5** 4700
[34] Hellman F, Hoffmann A, Tserkovnyak Y, *et al.* 2017 *Rev. Mod. Phys.* **89** 025006
[35] Arias R and Mills D L 1999 *Phys. Rev. B* **60** 7395
[36] Bergmann K von, Kubetzka A, Pietzsch O and Wiesendanger R 2014 *J. Phys. Condens. Matter.* **26** 394002
[37] Bousquet E and Cano A 2016 *J. Phys. Condens. Matter.* **28** 123001
[38] Kitaev A 2006 *Ann Phys.* **321** 2
[39] Takagi H, Takayama T, Jackeli G, Khaliullin G and Nagler S E 2019 *Nat. Rev. Phys.* **1** 264
[40] Winter S M, Tsirlin A A, Daghofer M, Brink J van den, Singh Y, Gegenwart P and Valenti R 2017 *J. Phys. Condens. Matter.* **29** 493002
[41] Trebst S and Hickey C 2022 *Phys. Rep.* **950** 1
[42] Kosterlit J M 1973 *J. Phys. C.* **6** 1181
[43] Kosterlitz J M 1974 *J. Phys. C Solid State Phys.* **7** 1046
[44] Berezinskii V L 1972 *Sov Phys. JETP.* **34** 610
[45] Kittel C 1987 *Quantum theory of solids* (Second Edition) p. 49
[46] Holstein T and Primakoff H 1940 *Phys. Rev.* **58** 1098
[47] Mermin N D and Wagner H 1966 *Phys. Rev. Lett.* **17** 1133
[48] Bogoljubov N N, Tolmachov V V and Širkov D 1958 *Fortschritte Phys.* **6** 605
[49] Johnston D C 2017 *Phys. Rev. B* **95** 094421
[50] Gomonay O, Baltz V, Brataas A and Tserkovnyak Y 2018 *Nat. Phys.* **14** 213
[51] Prosnikov M A, Smirnov A N, Davydov V Yu, Pisarev R V, Lyubochko N A and Barilo S N 2018 *Phys. Rev. B* **98** 104404
[52] Fulara H, Zahedinejad M, Khymyn R, Awad A A, Muralidhar S, Dvornik M, and Åkerman J 2019 *Sci. Adv.* **5** eaax8467
[53] Lebrun R, Ross A, Bender S A, Qaiumzadeh A, Baldrati L, Cramer J, Brataas A, Duine R A and Kläui M 2018 *Nature* **561** 222
[54] Holanda J, Maior D S, Azevedo A and Rezende S M 2018 *Nat. Phys.* **14** 500
[55] Němec P, Fiebig M, Kampfrath T and Kimel A V 2018 *Nat. Phys.* **14** 229
[56] Baltz V, Manchon A, Tsoi M, Moriyama T, Ono T and Tserkovnyak Y 2018 *Rev. Mod. Phys.* **90** 015005
[57] Bae Y J, Wang J, Scheie A, Xu J, Chica D G, Diederich G M, Cenker J, Ziebel M E, Bai Y, Ren H, Dean C R, Delor M, Xu X, Roy X, Kent A D and Zhu X 2022 *Nature* **609** 282
[58] Scheie A, Ziebel M, Chica D G, Bae Y J, Wang X, Kolesnikov A I, Zhu X and Roy X 2022 *Adv. Sci.* **9** 2202467
[59] Wildes A R, Rule K C, Bewley R I, Enderle M and Hicks T J 2012 *J. Phys. Condens. Matter.* **24** 416004
[60] Jin W, Kim H H, Ye Z, Li S, Rezaie P, Diaz F, Siddiq S, Wauer E, Yang B, Li C, Tian S, Sun K, Lei H, Tsen A W, Zhao L and He R 2018 *Nat. Commun.* **9** 5122
[61] Rudziński W 2022 *J. Magn. Magn. Mater.* **546** 168687
[62] Do S H, Kaneko K, Kajimoto R, Kamazawa K, Stone M B, Lin J Y Y, Itoh S, Masuda T, Samolyuk G D, Dagotto E, Meier W R, Sales B C, Miao H and Christianson A D 2022 *Phys. Rev. B* **105** L180403
[63] Lyu B, Gao Y, Zhang Y, Wang L, Wu X, Chen Y, Zhang J, Li G, Huang Q, Zhang N, Chen Y, Mei J, Yan H, Zhao Y, Huang L and Huang M 2020 *Nano Lett.* **20** 6024
[64] Hovancik D, Repcek D, Borodavka F, Kadlec C, Dolezal P, Kratochvilova M, Kuzel P, Kamba S, Sechovsky V and Pospisil J 2022 *J. Phys. Chem. Lett.* **13** 11095
[65] Do S H, Paddison J A M, Sala G, Williams T J, Kaneko K, Kuwahara K, May A F, Yan J, McGuire M A, Stone M B, Lumsden M D and Christianson A D 2022 *Phys. Rev. B* **106** L060408
[66] MacNeill D, Hou J T, Klein D R, Zhang P, Jarillo-Herrero P and Liu L 2019 *Phys. Rev. Lett.* **123** 047204
[67] Kim H H, Yang B, Li S, Jiang S, Jin C, Tao Z, Nichols G, Sfigakis F, Zhong S, Li C, Tian S, Cory D G, Miao G X, Shan J, Mak K F, Lei H, Sun K, Zhao L and Tsen A W 2019 *Proc. Natl. Acad. Sci. USA* **116** 11131
[68] Schneeloch J A, Tao Y, Cheng Y, Daemen L, Xu G, Zhang Q and Louca D 2022 *Npj Quantum Mater.* **7** 66
[69] Nikitin S E, Fåk B, Krämer K W, Fennell T, Normand B, Läuchli A M and Rüegg C 2022 *Phys. Rev. Lett.* **129** 127201
[70] Cai Z, Bao S, Gu Z L, *et al.* 2021 *Phys. Rev. B* **104** L020402
[71] Ghazaryan D, Greenaway M T, Wang Z, Guarochico-Moreira V H, Vera-Marun I J, Yin J, Liao Y, Morozov S V, Kristanovski O, Lichtenstein A I, Katsnelson M I, Withers F, Mishchenko A, Eaves L, Geim A K, Novoselov K S and Misra A 2018 *Nat. Electron.* **1** 344
[72] Schneeloch J A, Tao Y, Cheng Y, Daemen L, Xu G, Zhang Q and Louca D 2022 *Npj Quantum Mater.* **7** 66
[73] Cenker J, Huang B, Suri N, Thijssen P, Miller A, Song T, Taniguchi T, Watanabe K, McGuire M A, Xiao D and Xu X 2021 *Nat. Phys.* **17** 20
[74] Zhang X X, Li L, Weber D, Goldberger J, Mak K F and Shan J 2020 *Nat. Mater.* **19** 838
[75] Li S, Ye Z, Luo X, Ye G, Kim H H, Yang B, Tian S, Li C, Lei H, Tsen A W, Sun K, He R and Zhao L 2020 *Phys. Rev. X* **10** 011075
[76] Klein D R, MacNeill D, Lado J L, Soriano D, Navarro-Moratalla E, Watanabe K, Taniguchi T, Manni S, Canfield P, Fernández-Rossier J and Jarillo-Herrero P 2018 *Science* **360** 1218

[77] Xu C, Carnahan C, Zhang H, Sretenovic M, Zhang P, Xiao D and Ke X 2023 *Phys. Rev. B* **107** L060404

[78] Kim C, Kim S, Park P, Kim T, Jeong J, Ohira-Kawamura S, Murai N, Nakajima K, Chernyshev A L, Mourigal M, Kim S J and Park J G 2023 *Nat. Phys.* **19** 1624

[79] Luo T, Ilyas B, Hoegen A V, Lee Y, Park J, Park J G and Gedik N 2024 *Nat. Commun.* **15** 2276

[80] Kim J H, Jung T S, Lee Y, Kim C, Park J G and Kim J H 2023 *Phys. Rev. B* **108** 064414

[81] Liu H, Wang X, Wu J, Chen Y, Wan J, Wen R, Yang J, Liu Y, Song Z and Xie L 2020 *ACS Nano* **14** 10544

[82] Occhialini C A, Tseng Y, Elnaggar H, Song Q, Blei M, Tongay S A, Bisogni V, De Groot F M F, Pelliciari J and Comin R 2024 *Phys. Rev. X* **14** 031007

[83] Zhu F, Zhang L, Wang X, Dos Santos F J, Song J, Mueller T, Schmalzl K, Schmidt W F, Ivanov A, Park J T, Xu J, Ma J, Lounis S, Blügel S, Mokrousov Y, Su Y and Brückel T 2021 *Sci. Adv.* **7** eabi7532

[84] Chen L, Mao C, Chung J H, Stone M B, Kolesnikov A I, Wang X, Murai N, Gao B, Delaire O and Dai P 2022 *Nat. Commun.* **13** 4037

[85] Liu C, Li Z, Hu J, Duan H, Wang C, Cai L, Feng S, Wang Y, Liu R, Hou D, Liu C, Zhang R, Zhu L, Niu Y, Zakharov A A, Sheng Z and Yan W 2023 *Adv. Mater.* **35** 2300247

[86] Wang Z, Zhang X X, Shiomi Y, Arima T hisa, Nagaosa N, Tokura Y and Ogawa N 2023 *Phys. Rev. Res.* **5** L042032

[87] Chen G, Qi S, Liu J, Chen D, Wang J, Yan S, Zhang Y, Cao S, Lu M, Tian S, Chen K, Yu P, Liu Z, Xie X C, Xiao J, Shindou R and Chen J H 2021 *Nat. Commun.* **12** 6279

[88] Wildes A R, Okamoto S and Xiao D 2021 *Phys. Rev. B* **103** 024424

[89] Vaclavkova D, Delhomme A, Faugeras C, Potemski M, Bogucki A, Suffczyński J, Kossacki P, Wildes A, Gremaud B and Saúl A 2020 *2D Mater.* **7** 035030

[90] Kim K, Lim S Y, Kim J, Lee J U, Lee S, Kim P, Park K, Son S, Park C H, Park J G and Cheong H 2019 *2D Mater.* **6** 041001

[91] Xing W, Qiu L, Wang X, Yao Y, Ma Y, Cai R, Jia S, Xie X C and Han W 2019 *Phys. Rev. X* **9** 011026

[92] Liao J, Huang Z, Shangguan Y, Zhang B, Cheng S, Xu H, Kajimoto R, Kamazawa K, Bao S and Wen J 2024 *Phys. Rev. B* **109** 224411

[93] Gillard D J, Wolverson D, Hutchings O M and Tartakovskii A I 2024 *Npj 2D Mater. Appl.* **8** 6

[94] Mai T T, Garrity K F, McCreary A, Argo J, Simpson J R, Doan-Nguyen V, Aguilar R V and Walker A R H 2021 *Sci. Adv.* **7** eabj3106

[95] Liu P, Xu Z, Huang H, Li J, Feng C, Huang M, Zhu M, Wang Z, Zhang Z, Hou D, Lu Y and Xiang B 2020 *J. Alloys Compd.* **828** 154432

[96] Kumar D, Hoang N T, Sim Y, Choi Y, Raju K, Ulaganathan R K, Sankar R, Seong M J and Choi K Y 2024 *Phys. Rev. B* **110** 064414

[97] Jana D, Kapuscinski P, Mohelsky I, Vaclavkova D, Breslavetz I, Orlita M, Faugeras C and Potemski M 2023 *Phys. Rev. B* **108** 115149

[98] Wildes A, Rule K, Bewley R, Enderle M and Hicks T 2012 *J. Phys. Condens Matter.* **24** 416004

[99] Pawbake A, Pelini T, Delhomme A, Romanin D, Vaclavkova D, Martinez G, Calandra M, Measson M A, Veis M, Potemski M, Orlita M and Faugeras C 2022 *ACS Nano* **16** 12656

[100] Luo J, Li S, Ye Z, Xu R, Yan H, Zhang J, Ye G, Chen L, Hu D, Teng X, Smith W A, Yakobson B I, Dai P, Nevidomskyy A H, He R and Zhu H 2023 *Nano Lett.* **23** 2023

[101] Sun Y J, Lai J M, Pang S M, Liu X L, Tan P H and Zhang J 2022 *J. Phys. Chem Lett.* **13** 1533

[102] Vaclavkova D, Palit M, Wyzula J, Ghosh S, Delhomme A, Maity S, Kapuscinski P, Ghosh A, Veis M, Grzeszczyk M, Faugeras C, Orlita M, Datta S and Potemski M 2021 *Phys. Rev. B* **104** 134437

[103] Liu S, Granados Del Águila A, Bhowmick D, Gan C K, Thu Ha Do T, Prosnikov M A, Sedmidubský D, Sofer Z, Christianen P C M, Sengupta P, and Xiong Q 2021 *Phys. Rev. Lett.* **127** 097401

[104] Ghosh A, Palit M, Maity S, Dwij V, Rana S and Datta S 2021 *Phys. Rev. B* **103** 064431

[105] Kargar F, Aytan E, Ghosh S, Lee J, Gomez M, Liu Y, Magana A S, Beiranvand Z B, Debnath B, Wilson R, Lake R K and Balandin A A 2020 *ACS Nano* **14** 2424

[106] McCreary A, Simpson J R, Mai T T, McMichael R D, Douglas J E, Butch N, Dennis C, Valdés Aguilar R and Hight Walker A R 2020 *Phys. Rev. B* **101** 064416

[107] Lee J U, Lee S, Ryoo J H, Kang S, Kim T Y, Kim P, Park C H, Park J G and Cheong H 2016 *Nano Lett.* **16** 7433

[108] Lançon D, Walker H C, Ressouche E, Ouladdiaf B, Rule K C, McIntyre G J, Hicks T J, Rønnow H M and Wildes A R 2016 *Phys. Rev. B* **94** 214407

[109] Mardele F L, Mendili A E, Zhitomirsky M E, Mohelsky I, Jana D, Plutnarova I, Sofer Z, Faugeras C, Potemski M and Orlita M 2024 *Phys. Rev. B* **109** 134410

[110] Cui J, Boström E V, Ozerov M, Wu F, Jiang Q, Chu J H, Li C, Liu F, Xu X, Rubio A and Zhang Q 2023 *Nat. Commun.* **14** 3396

[111] Luo J, Li S, Ye Z, Xu R, Yan H, Zhang J, Ye G, Chen L, Hu D, Teng X, Smith W A, Yakobson B I, Dai P, Nevidomskyy A H, He R and Zhu H 2023 *Nano Lett.* **23** 2023

[112] Kim C, Jeong J, Masuda T, Asai S, Itoh S, Kim H S, Wildes A and Park J G 2020 *Phys. Rev. B* **102** 184429

[113] Liu Q, Wang L, Fu Y, Zhang X, Huang L, Su H, Lin J, Chen X, Yu D, Cui X, Mei J W and Dai J F 2021 *Phys. Rev. B* **103** 235411

[114] Rosenblum S, Francis A H and Merlin R 1994 *Phys. Rev. B* **49** 4352

[115] Rosenblum S S and Merlin R 1999 *Phys. Rev. B* **59** 6317

[116] Fei F, Mao Y, Fang W, Liu W, Rollins J P, Kondusamy A L N, Lv B, Ping Y, Wang Y and Xiao J 2024 *Nano Lett.* **24** 10467

[117] Bae Y J, Handa T, Dai Y, Wang J, Liu H, Scheie A, Chica D G, Ziebel M E, Kent A D, Xu X, Shen K, Roy X and Zhu X 2024 *Phys. Rev. B* **109** 104401

[118] Cho C W, Pawbake A, Aubergier N, Barra A L, Mosina K, Sofer Z, Zhitomirsky M E, Faugeras C and Piot B A 2023 *Phys. Rev. B* **107** 094403

[119] Pawbake A, Pelini T, Wilson N P, Mosina K, Sofer Z, Heid R and Faugeras C 2023 *Phys. Rev. B* **107** 075421

[120] Diederich G M, Cenker J, Ren Y, Fonseca J, Chica D G, Bae Y J, Zhu X, Roy X, Cao T, Xiao D and Xu X 2023 *Nat. Nanotechnol.* **18** 23

[121] Cham T M J, Karimeddiny S, Dismukes A H, Roy X, Ralph D C and Luo Y K 2022 *Nano Lett.* **22** 6716

[122] Chen J, Yuan R, Yu K, Wang X, Sheng L, Wang J, Hua C, Yu W, Xiao J, Liu S, Yu D, Ansermet J P, Wang Z and Yu H 2025 *Appl Phys. Rev.* **12** 011407

[123] De Wal D K, Mena R L, Zohaib M and Van Wees B J 2024 *Phys. Rev. B* **110** 224434

[124] De Wal D K, Zohaib M and Van Wees B J 2024 *Phys. Rev. B* **110** 174440

[125] Wal D K de, Iwens A, Liu T, Tang P, Bauer G E W and Wees B J van 2023 *Phys. Rev. B* **107** L180403

[126] Qi S, Chen D, Chen K, *et al*. 2023 *Nat. Commun.* **14** 2526

[127] Lujan D, Choe J, Rodriguez-Vega M, Ye Z, Leonardo A, Nunley T N, Chang L J, Lee S F, Yan J, Fiete G A, He R and Li X 2022 *Nat. Commun.* **13** 2527

[128] Vu D D, Nelson R A, Wooten B L, Barker J, Goldberger J E and Heremans J P 2023 *Phys. Rev. B* **108** 144402

[129] Bartram F M, Li M, Liu L, Xu Z, Wang Y, Che M, Li H, Wu Y, Xu Y, Zhang J, Yang S and Yang L 2023 *Sci. Bull.* **68** 2734

[130] Yang B, Goh Y M, Sung S H, Ye G, Biswas S, Kaib D A S, Dhakal R, Yan S, Li C, Jiang S, Chen F, Lei H, He R, Valentí R, Winter S M, Hovden R and Tsen A W 2023 *Nat. Mater.* **22** 50

[131] Wulferding D, Choi Y, Do S H, Lee C H, Lemmens P, Faugeras C, Gallais Y and Choi K Y 2020 *Nat. Commun.* **11** 1603

[132] Balz C, Lampen-Kelley P, Banerjee A, Yan J, Lu Z, Hu X, Yadav S M, Takano Y, Liu Y, Tennant D A, Lumsden M D, Mandrus D and Nagler S E 2019 *Phys. Rev. B* **100** 060405

[133] Ozel I O, Belvin C A, Baldini E, Kimchi I, Do S, Choi K Y and Gedik N 2019 *Phys. Rev. B* **100** 085108

[134] Shi L Y, Liu Y Q, Lin T, Zhang M Y, Zhang S J, Wang L, Shi Y G, Dong T and Wang N L 2018 *Phys. Rev. B* **98** 094414

[135] Choi Y, Lee J H, Lee S, Wulferding D, Fujihara H, Sato F, Imai Y, Ohgushi K, Seong M J and Choi K Y 2022 *Phys. Rev. B* **106** 174430

[136] Bae Y J, Handa T, Dai Y, Wang J, Liu H, Scheie A, Chica D G, Ziebel M E, Kent A D, Xu X, Shen K, Roy X and Zhu X 2024 *Phys. Rev. B* **109** 104401

[137] Cui Q, Bai X and Delin A 2025 *Adv. Funct. Mater.* **35** 2407469

[138] Soenen M, Bacaksiz C, Menezes R M and Milosevic M V 2023 *Phys. Rev. Mater.* **7** 024421

[139] Kim H H, Yang B, Li S, Jiang S, Jin C, Tao Z, Nichols G, Sfigakis F, Zhong S, Li C, Tian S, Cory D G, Miao G X, Shan J, Mak K F, Lei H, Sun K, Zhao L and Tsen A W 2019 *Proc. Natl. Acad. Sci. USA* **116** 11131

[140] Chen L, Chung J H, Stone M B, Kolesnikov A I, Winn B, Garlea V O, Abernathy D L, Gao B, Augustin M, Santos E J G and Dai P 2021 *Phys. Rev. X* **11** 031047

[141] Lee I, Utermohlen F G, Weber D, Hwang K, Zhang C, Van Tol J, Goldberger J E, Trivedi N and Hammel P C 2020 *Phys. Rev. Lett.* **124** 017201

[142] Diederich G M, Cenker J, Ren Y, Fonseca J, Chica D G, Bae Y J, Zhu X, Roy X, Cao T, Xiao D and Xu X 2023 *Nat. Nanotechnol.* **18** 23

[143] Na W, Park P, Oh S, Kim J, Scheie A, Tennant D A, Lee H C, Park J G and Cheong H 2024 *ACS Nano* **18** 20482

[144] Cui J, Boström E V, Ozerov M, Wu F, Jiang Q, Chu J H, Li C, Liu F, Xu X, Rubio A and Zhang Q 2023 *Nat. Commun.* **14** 3396

[145] Jana D, Kapuściński P, Pawbake A, Papavasileiou A, Sofer Z, Breslavetz I, Orlita M, Potemski M and Faugeras C 2023 *Phys. Rev. B* **108** 144415

[146] Mai T T, Garrity K F, McCreary A, Argo J, Simpson J R, Doan-Nguyen V, Aguilar R V and Walker A R H 2021 *Sci. Adv.* **7** eabj3106

[147] Seo J, Kim D Y, An E S, *et al*. 2020 *Sci. Adv.* **6** eaay8912

[148] Deng Y, Yu Y, Song Y, Zhang J, Wang N Z, Sun Z, Yi Y, Wu Y Z, Wu S, Zhu J, Wang J, Chen X H and Zhang Y 2018 *Nature* **563** 94

[149] Deng Y, Yu Y, Shi M Z, Guo Z, Xu Z, Wang J, Chen X H and Zhang Y 2020 *Science* **367** 895

[150] Li B, Pajerowski D M, Riberolles S X M, Ke L, Yan J Q and McQueeney R J 2021 *Phys. Rev. B* **104** L220402

[151] Zhang Y, Gu Y, Weng H, Jiang K and Hu J 2023 *Phys. Rev. B* **107** 035126

[152] Nakamura R, Takegami D, Fujinuma K, Nakamura M, Ferreira-Carvalho M, Melendez-Sans A, Yoshimura M, Tsuei K D, Haraguchi Y, Aruga Katori H, Tjeng L H and Mizokawa T 2024 *Phys. Rev. B* **110** L081109

[153] Haraguchi Y, Michioka C, Ishikawa M, Nakano Y, Yamochi H, Ueda H and Yoshimura K 2017 *Inorg Chem.* **56** 3483

[154] Feng Z, Li Z, Meng X, Yi W, Wei Y, Zhang J, Wang Y C, Jiang W, Liu Z, Li S, Liu F, Luo J, Li S, Zheng G qing, Meng Z Y, Mei J W and Shi Y 2017 *Chin. Phys. Lett.* **34** 077502

[155] Rossat-Mignod J, Regnault L P, Vettier C, Burlet P, Henry J Y and Lapertot G 1991 *Phys. B* **169** 58

[156] Hudson B S 2006 *Vib Spectrosc.* **42** 25

[157] Pintschovius L 2005 *Phys. Status Solidi B* **242** 30

[158] Lai J M, Xie Y R and Zhang J 2021 *Nano Res.* **14** 1711

[159] Lai J M, Farooq M U, Sun Y J, Tan P H and Zhang J 2022 *Nano Lett.* **22** 5385

[160] Lai J M, Xie Y R and Zhang J 2021 *Nano Res.* **14** 1711

[161] Li B, Xing T, Zhong M, Huang L, Lei N, Zhang J, Li J and Wei Z 2017 *Nat. Commun.* **8** 1958

[162] Gu P, Tan Q, Wan Y, Li Z, Peng Y, Lai J, Ma J, Yao X, Yang S, Yuan K, Sun D, Peng B, Zhang J and Ye Y 2020 *ACS Nano.* **14** 1003

[163] Fleury P A and Loudon R 1968 *Phys. Rev.* **166** 514

[164] Pang S M, Xie Y R, Shen C and Zhang J 2023 *J. Phys. Chem. Lett.* **14** 6977

[165] Pang S M, Lv Y P and Zhang J 2024 *J. Raman Spectrosc.* **55** 1019

[166] Pang S, Liu X, Luo J, Xie Y, Tang J, Meng S, Tan P H and Zhang J 2022 *Adv. Photonics Res.* **3** 2100222

[167] Xie Y, Ren S, Gao Y, Liu X, Tan P and Zhang J 2021 *Sci. China Phys. Mech. Astron.* **64** 287311

[168] Kargar F and Balandin A A 2021 *Nat. Photonics* **15** 720

[169] Ren S, Pang S, Guan S, Sun Y J, Zhang T Y, Jiang N, Guo J, Zheng H, Luo J W, Tan P H, Shen C and Zhang J 2025 *Nano Lett.* **25** 2709

[170] Ren S, Liu C, Xu K, Jiang N, Hu F, Tan P H, Zheng H, Xu X, Shen C and Zhang J 2022 *J. Phys. Chem Lett.* **13** 1697

[171] Huang B, Clark G, Navarro-Moratalla E, Klein D R, Cheng R, Seyler K L, Zhong D, Schmidgall E, McGuire M A, Cobden D H, Yao W, Xiao D, Jarillo-Herrero P and Xu X 2017 *Nature* **546** 270

[172] Zhang H, Ni Z, Stevens C E, Bai A, Peiris F, Hendrickson J R, Wu L and Jariwala D 2022 *Nat. Photonics.* **16** 311

[173] Hwangbo K, Zhang Q, Jiang Q, Wang Y, Fonseca J, Wang C, Diederich G M, Gamelin D R, Xiao D, Chu J H, Yao W and Xu X 2021 *Nat. Nanotechnol.* **16** 655

[174] Jiang S, Shan J and Mak K F 2018 *Nat. Mater.* **17** 406

[175] Liu S, Granados Del Águila A, Bhowmick D, Gan C K, Thu Ha Do T, Prosnikov M A, Sedmidubský D, Sofer Z, Christianen P C M, Sengupta P, and Xiong Q 2021 *Phys. Rev. Lett.* **127** 097401

[176] Mai T T, Garrity K F, McCreary A, Argo J, Simpson J R, Doan-Nguyen V, Aguilar R V and Walker A R H 2021 *Sci. Adv.* **7** eabj3106

[177] De Wal D K, Mena R L, Zohaib M and Van Wees B J 2024 *Phys. Rev. B* **110** 224434

[178] De Wal D K, Zohaib M and Van Wees B J 2024 *Phys. Rev. B* **110** 174440

[179] Chen G, Qi S, Liu J, Chen D, Wang J, Yan S, Zhang Y, Cao S, Lu M, Tian S, Chen K, Yu P, Liu Z, Xie X C, Xiao J, Shindou R and Chen J H 2021 *Nat. Commun.* **12** 6279

[180] Qi S, Chen D, Chen K, *et al*. 2023 *Nat. Commun.* **14** 2526

[181] Sun Y, Lin T, Lei N, *et al*. 2023 *Nat. Commun.* **14** 3434

[182] Kosevich A M, Ivanov B A and Kovalev A S 1990 *Phys. Rep.* **194** 117

[183] Sulymenko O R, Prokopenko O V, Tyberkevych V S, Slavin A N and Serga A A 2018 *Low Temp. Phys.* **44** 602

[184] Elyasi M, Sato K and Bauer G E W 2019 *Phys. Rev. B* **99** 134402

[185] Büttner O, Bauer M, Demokritov S O, Hillebrands B, Kivshar Yu S, Grimalsky V, Rapoport Yu, Kostylev M P, Kalinikos B A and Slavin A N 2000 *J. Appl. Phys.* **87** 5088

[186] Slavin A N and Rojdestvenski I V 1994 *IEEE Trans Magn.* **30** 37

[187] Leykam D and Chong Y D 2016 *Phys. Rev. Lett.* **117** 143901

[188] Šmejkal L, Marmodoro A, Ahn K H, González-Hernández R, Turek I, Mankovsky S, Ebert H, D'Souza S W, Šipr O, Sinova J and Jungwirth T 2023 *Phys. Rev. Lett.* **131** 256703

[189] Wang Q, Wu D W, Guo G H, Long M Q and Wang Y P 2024 *Chin. Phys. B* **33** 097507

[190] Motome Y and Nasu J 2020 *J. Phys. Soc Jpn.* **89** 012002

[191] Burch K S, Mandrus D and Park J G 2018 *Nature* **563** 47

[192] Li Z, Lai J and Zhang J 2022 *J. Semicond.* **44** 011902

[193] Kim K M, Kiem D H, Bednik G, Han M J and Park M J 2023 *Nano Lett.* **23** 6088

[194] Wang C, Gao Y, Lv H, Xu X and Xiao D 2020 *Phys. Rev. Lett.* **125** 247201

[195] DiScala M F, Staros D, Torre A de la, Lopez A, Wong D, Schulz C, Bartkowiak M, Rubenstein B and Plumb K W 2024 *Adv. Phys. Res.* **3** 2300096

[196] Song T, Sun Q C, Anderson E, Wang C, Qian J, Taniguchi T, Watanabe K, McGuire M A, Stöhr R and Xiao D 2021 *Science* **374** 1140

[197] Adhikari K, Choudhury S, Barman S, Otani Y and Barman A 2021 *Nanotechnology* **32** 395706

[198] Zhou J, Lu H, Chen D, Huang M, Yan G Q, Al-matouq F, Chang J, Djugba D, Jiang Z, Wang H and Du C R 2024 *Sci. Adv.* **10** eadk8495

[199] Ho K O, Shen Y, Pang Y Y, Leung W K, Zhao N and Yang S 2021 *Funct. Diam.* **1** 160

[200] Xu Y, Zhang W and Tian C 2023 *Photonics Res.* **11** 393

[201] Wang C J, Shi F Z, Wang P F, Duan C K and Du J F 2018 *Acta Phys. Sin.* **67** 130701 (in Chinese)

[202] Zhang J, Lai J M 2020 *Journal of Northwest University* (natural science edition) **50**: 338

[203] Pang S M, Xie Y R and Zhang J 2021 *The Journal of Light Scattering* **33** 101